Article:
Foster, Simon, Lund, Victoria A, Wacnik, Katarzyna et al. (11 more authors) (2018) Molecular coordination of Staphylococcus aureus cell division. eLife. pp. 1-31. ISSN: 2050-084X

https://doi.org/10.7554/eLife.32057.001

24 Hills Road, **P** 01223 855346
Cambridge **W** elifesciences.org
CB2 1JP **T** @elife_sciences

Molecular coordination of *Staphylococcus aureus* cell division

Tracking no: 15-09-2017-RA-eLife-32057R2

Simon Foster (University of Sheffield), Victoria Lund (University of Sheffield), Katarzyna Wacnik (University of Sheffield), Robert Turner (University of Sheffield), Bryony Cotterell (University of Sheffield), Christa Walther (University of Sheffield), Samuel Fenn (University of Sheffield), Fabian Grein (University of Bonn), Adam Wollman (University of York), Mark Leake (University of York), Nicolas Olivier (University of Sheffield), Ashley Cadby (University of Sheffield), Stephane Mesnage (University of Sheffield), and Simon Jones (University of Sheffield)

Abstract:
The bacterial cell wall is essential for viability, but despite its ability to withstand internal turgor must remain dynamic to permit growth and division. Peptidoglycan is the major cell wall structural polymer, whose synthesis requires multiple interacting components. The human pathogen *Staphylococcus aureus* is a prolate spheroid that divides in three orthogonal planes. Here, we have integrated cellular morphology during division with molecular level resolution imaging of peptidoglycan synthesis and the components responsible. Synthesis occurs across the developing septal surface in a diffuse pattern, a necessity of the observed septal geometry, that is matched by variegated division component distribution. Synthesis continues after septal annulus completion, where the core division component FtsZ remains. The novel molecular level information requires re-evaluation of the growth and division processes leading to a new conceptual model, whereby the cell cycle is expedited by a set of functionally connected but not regularly distributed components.

Impact statement: Morphological constraints dictate division mode in the human pathogen Staphylococcus aureus

Competing interests: No competing interests declared

Author contributions:
Simon Foster: Conceptualization; Formal analysis; Supervision; Funding acquisition; Investigation; Project administration; Writing—review and editing Victoria Lund: Conceptualization; Data curation; Formal analysis; Investigation; Methodology; Writing—original draft; Writing—review and editing Katarzyna Wacnik: Conceptualization; Data curation; Formal analysis; Investigation; Methodology; Writing—original draft; Writing—review and editing Robert Turner: Conceptualization; Data curation; Software; Formal analysis; Validation; Investigation; Methodology; Writing—original draft; Writing—review and editing Bryony Cotterell: Resources; Formal analysis; Investigation; Methodology; Writing—review and editing Christa Walther: Formal analysis; Investigation; Methodology; Writing—review and editing Samuel Fenn: Data curation; Methodology Fabian Grein: Resources; Data curation; Methodology Adam Wollman: Formal analysis; Methodology; Writing—review and editing Mark Leake: Conceptualization; Supervision; Funding acquisition; Project administration; Writing—review and editing Nicolas Olivier: Methodology; Writing—review and editing Ashley Cadby: Supervision; Methodology; Writing—review and editing Stephane Mesnage: Formal analysis; Methodology; Writing—review and editing Simon Jones: Formal analysis; Supervision; Funding acquisition; Project administration; Writing—review and editing

Funding:
RCUK | Medical Research Council (MRC): Simon J Foster, MR/N002679/1; RCUK | Biotechnology and Biological Sciences Research Council (BBSRC): Simon J Foster, BB/L006162/1; RCUK | Medical Research Council (MRC): Simon J Foster, MR/K015753/1; RCUK | Medical Research Council (MRC): Simon J Foster, G1100127; RCUK | Medical Research Council (MRC): Mark C Leake, MR/K01580X/1; RCUK | Biotechnology and Biological Sciences Research Council (BBSRC): Mark C Leake, BB/N006453/1 The funders had no role in study design, data collection and interpretation, or the decision to submit the work for publication.

Datasets:
N/A

Ethics:
Human Subjects: No Animal Subjects: No

Author Affiliation:
Simon Foster(Krebs Institute,University of Sheffield,United Kingdom) Victoria Lund(Krebs Institute,University of Sheffield,United Kingdom)

Katarzyna Wacnik(Krebs Institute,University of Sheffield,United Kingdom) Robert Turner(Krebs Institute,University of Sheffield,United Kingdom) Bryony Cotterell(Krebs Institute,University of Sheffield,United Kingdom) Christa Walther(Krebs Institute,University of Sheffield,United Kingdom) Samuel Fenn(Krebs Institute,University of Sheffield,United Kingdom) Fabian Grein(Institute for Pharmaceutical Microbiology,University of Bonn,Germany) Adam Wollman(Biological Physical Sciences Institute,University of York,United Kingdom) Mark Leake(Biological Physical Sciences Institute,University of York,United Kingdom) Nicolas Olivier(Krebs Institute,University of Sheffield,United Kingdom) Ashley Cadby(Krebs Institute,University of Sheffield,United Kingdom) Stephane Mesnage(Krebs Institute,University of Sheffield,United Kingdom) Simon Jones(Chemistry,University of Sheffield,United Kingdom)

Dual-use research: No

Permissions: Have you reproduced or modified any part of an article that has been previously published or submitted to another journal? No

Molecular coordination of *Staphylococcus aureus* cell division

Victoria A. Lund[1,2,†], Katarzyna Wacnik[1,2,†], Robert D. Turner[1,2,3,†], Bryony E. Cotterell[1,2,4], Christa G. Walther[1,2],Samuel J Fenn[1,2], Fabian Grein[5], Adam J. M. Wollman[6], Mark C. Leake[6], Nicolas Olivier[1,3], Ashley Cadby[1,3], Stéphane Mesnage[1,2], Simon Jones[1,4], Simon Foster[1,2,]*

[1] Krebs Institute, University of Sheffield, Firth Court, Western Bank, Sheffield, S10 2TN
[2] Department of Molecular Biology & Biotechnology, University of Sheffield, Firth Court, Western Bank, Sheffield, S10 2TN
[3] Department of Physics and Astronomy, University of Sheffield, Hicks Building, Hounsfield Road, Sheffield, S3 7RH
[4] Department of Chemistry, University of Sheffield, Dainton Building, Brook Hill Sheffield, S3 7HF
[5] University of Bonn, University Clinic, Institute for Pharmaceutical Microbiology, Meckenheimer Allee 168, 53115, Bonn, Germany and German Center for Infection Research (DZIF), partner site Bonn-Cologne, Bonn, Germany
[6] Biological Physical Sciences Institute, University of York, York, YO10 5DD, UK
* Corresponding Author
† These authors contributed equally

Abstract

The bacterial cell wall is essential for viability, but despite its ability to withstand internal turgor it must remain dynamic to permit growth and division. In most bacteria peptidoglycan is the major cell wall structural polymer, for which the advent of super resolution microscopy approaches has begun to reveal a complex architecture, whose synthesis requires multiple interacting components. The human pathogen *Staphylococcus aureus* is a prolate spheroid that divides in three orthogonal planes, requiring intricate spatio-temporal process control to complete the cell cycle with fidelity. Here, we have integrated cellular morphology during division with molecular level resolution imaging of peptidoglycan synthesis and the components responsible. Synthesis occurs across the developing septal surface in a diffuse pattern, a necessity of the observed septal geometry, that is matched by a variegated division component distribution. Synthesis continues after septal annulus completion, where the core division component FtsZ remains. The combination of molecular level information requires a re-evaluation of the growth and division processes leading to the development of a new conceptual model, whereby the cell cycle is expedited by a set of functionally connected but not regularly distributed components.

Significance Statement

Bacterial cell wall peptidoglycan is responsible for maintaining viability, acting as a physical “exoskeleton” and its synthesis is the target of some of the most important antibiotics such as penicillin and vancomycin. Despite this we understand little of how this essential polymer is made and the organisation of the complex set of components required during growth and division. We have used molecular level resolution microscopy to map both peptidoglycan production and the major proteins involved, in the important human

pathogen, *Staphylococcus aureus*. This has revealed unprecedented detail and an unexpected diffuse pattern of peptidoglycan synthesis during division, matched by the localisation of the components required. This has led to a new division model driven by cellular morphological constraints.

Introduction

In order to grow and divide, bacteria must make new cell wall, the major structural component of which is peptidoglycan (1). Bacteria generally have two groups of proteins that co-ordinate peptidoglycan insertion, one involved with elongation (elongasome), the other with division (divisome) (2). *S. aureus* lacks an apparent elongasome machinery, but nonetheless new peptidoglycan is inserted all over the cell surface, throughout the cell cycle, not just during cell division (3, 4). Addition of peptidoglycan, along with its hydrolysis (5), is what enables *S. aureus* cells to get bigger – volume increases at a constant rate (4).

The *S. aureus* divisome contains both enzymes that catalyse addition of new monomers to the peptidoglycan envelope (Penicillin Binding Proteins, PBPs), and proteins that co-ordinate this activity. Chief amongst these is FtsZ - an essential protein in almost all bacteria that directs cell division, which has recently been shown to form dynamic filaments that "treadmill" in *Escherichia coli* and *Bacillus subtilis*, giving a framework to assemble other division proteins resulting in cell wall biosynthesis and septum formation (6, 7). FtsZ assembly into the Z-ring is regulated by other cell division components including EzrA (8, 9), a membrane protein crucial for cell division in *S. aureus* (10). It has been shown to interact with both cytoplasmic proteins and those with periplasmic domains and it is therefore proposed to act as an interface between FtsZ and PBPs forming a scaffold for other cell division components (10).

Previously, FtsZ and EzrA in *S. aureus* have been imaged using fluorescent fusions (11, 12) and sites of peptidoglycan insertion using fluorescent D-amino acids (3, 13). Here we have applied single molecule localisation microscopy, a technique that provides unprecedented detail compared with other approaches. This has revealed an unexpected arrangement of division proteins and associated peptidoglycan insertion pattern. This defies the conventional view of division in *S. aureus* and has prompted a new model of division that encompasses the morphological idiosyncrasies of this important pathogen.

Results

Distribution of divisome components during septation

In order to visualise division machines, we localised the cytoplasmic initiator of division FtsZ and the crucial membrane protein EzrA (10).

Four fusions of EzrA with different fluorophores were created. These had wild-type growth rates and the previously observed septal EzrA localization pattern (10, 14) by diffraction limited microscopy (Fig. 1 - supplement 1). Localisation microscopy and 3D Structured Illumination Microscopy (3D-SIM) were used to address the distribution and juxtaposition of the cell division components at super-resolution.

3D-SIM revealed that EzrA exhibited punctate distribution at the division site (Fig. 1 – supplement 2a) (11). Unfortunately, the “honeycomb” artefact (which introduces foci in images due to incomplete noise filtering (15)) could not be removed by raising the Weiner filter parameter in reconstructions. Thus, localisation microscopy was employed as a superior approach.

eYFP was selected as a blinking fluorescent protein tag (16). Multiple 2D images of septa in the plane of focus were obtained for EzrA-eYFP (Fig. 1a), FtsZ-eYFP (Fig. 1b) and EzrA-meYFP (Fig. 1 - supplement 2b). The mean localisation precision of YFP was calculated using two different formulas: the “Thompson Equation” (17) by the ThunderSTORM ImageJ plugin yielded 24 (s.d. 8.5) nm while a using a modified version of this equation (18) yielded 27 (s.d. 8.7) nm. We also measured it experimentally using Nearest Neighbour in Adjacent Frames (NeNA) analysis (19): NeNA analysis determines localisation precision based on spatial proximity of blinks that occur at similar times and is part of a family of clustering-based tools for assessing the quality of localisation microscopy data (20). This method gave us a mean localization precision of 16.23 nm. Many of the septa appeared to be somewhat elliptical. This is likely due to the cells being tilted relative to the plane of focus leading to circular septa appearing elliptical. We therefore fitted ellipses to the septal localisations and calculated the expected tilt of the cells. The results were that all of the localisations included in our analysis are within a 400 nm optical section, within a range to ensure good data (21).

To analyse the distributions and address issues of sampling and resolution in our microscopy, a number of simple simulations were carried out where representative numbers of localisations were distributed at random in rings of similar radius to those observed, with a random error applied (Fig. 1c). A circle was fitted to the data points and all the distributions (experimental and simulated) were parameterised with respect to angle and distance from the centre of the circle, generating histograms of localisations (Fig. 1d, e). The autocorrelations of the angular distributions were then averaged to show that the localisations in the experimental data were neither completely randomly, or regularly, distributed around the ring (Fig. 1f). Distributions of distance from the centre of the circle were compared with simulated distributions of a fixed circle radius where different levels of localisation precision error were applied (Fig. 1g). Even with the most

conservative assumptions (including simulated localisation precisions worse than we had calculated for our measured data), the localisations were spread out over a sufficiently wide range of distances to indicate that both FtsZ or EzrA do not form a very thin ring at the leading edge of the septum in *S. aureus*. Instead both proteins appear in a non-uniform distribution within the septal annulus. Within the annulus the proteins show no discernible pattern within or across cells. FtsZ distributions were consistent with FtsZ remaining in the division plane after septal fusion were also observed (Fig. 2a).

To further investigate whether the apparent elliptical shape of the rings had an influence on our interpretation, we also analysed the data using an elliptical, rather than a circular fit. Comparing our results to simulated data (Fig. 1 – supplement 3) corroborated our previous findings.

To place these findings in the context of cell wall shape, two colour localisation microscopy was performed where the cell wall was labelled with an Alexa Fluor 647 NHS ester (Fig. 2b, c), which labels all amine groups in the cell wall (4). This confirmed that EzrA and FtsZ were at the expected septal positions in the cell.

To analyse rapid molecular dynamics of EzrA, single-molecule Slimfield microscopy (22) was performed on EzrA-meYFP labelled *S. aureus*, SH4604 (*ezrA-meyfp ΔezrA*) optimized to enable blur-free tracking of single fluorescent protein fusion constructs in live cells over a millisecond timescale (23, 24). Analysis of the mobility of tracked EzrA-meYFP foci enabled quantification of their microdiffusion coefficient (D), indicating a mixture of three different mobility components: an apparent immobile population in addition to an intermediate and a rapid mobility population (Fig. 1 – supplement 4a, b). In total, ~600 EzrA foci tracks were analysed in the septum region, whose overall mean D value, which captures both the immobile and two mobile populations, was 0.20±0.01 $\mu m^2 s^{-1}$. Whereas, 140 foci tracks were detected outside the septum region, which showed an increased overall mean D of 0.28±0.03 $\mu m^2 s^{-1}$. This greater average mobility was principally due to an increase in the proportion of EzrA foci present in the most mobile component (going from 33±3% of the total to 42±4%).

These relatively slow mobility values for EzrA, compared to many freely diffusing bacterial membrane integrated proteins (25), do not preclude putative rotational/treadmilling motions of EzrA (which have been observed in previous studies of FtsZ mobility in *E. coli* and *B. subtilis* (6, 7)) over a longer time scale. For example, the mean speed of putative FtsZ treadmilling estimated from *B. subtilis* recently (7) is only ~30nm/s, which we estimate would be sufficiently slow to appear predominantly in the immobile component over the typical time scales of our Slimfield tracking experiments here, and so putative

treadmilling of EzrA at this equivalent mean speed, if present in *S. aureus*, would most likely appear in this apparent immobile fraction. However, in the three component mobility model, which fits the observed distribution of D values well, the intermediate mobility fraction has been interpreted previously in other cellular systems as indicating transient dynamic interactions (26), and so we cannot entirely exclude the possibility that this may be due to transient association of EzrA with FtsZ. Deconvolution analysis (27) of whole cell images obtained using Slimfield microscopy indicated a mean total copy number of 305±23 EzrA molecules per cell measured across a population (Fig. 1 – supplement 4c). Estimating the proportion of the most mobile fraction of EzrA foci therefore indicates that at least ~100 EzrA molecules per cell are not likely to be treadmilling in tight association with FtsZ. In other words, we cannot account for the observed mobility of EzrA by a simple treadmilling model alone in which all EzrA is tightly associated to FtsZ, rather the real cellular behaviour is more complex than this.

Peptidoglycan synthesis in *S. aureus* does not occur in discrete foci

We used established metabolic labelling with fluorescent D-amino acids or dipeptides (3, 13) and adapted this for localisation microscopy in order to visualise peptidoglycan insertion with this higher resolution imaging technique. We confirmed that HADA (7-hydroxycoumarin-3-carboxylic acid-amino-D-alanine), ADA (azido D-alanine) and ADA-DA (azido-D-alanyl-D-alanine) mark regions of new peptidoglycan insertion by microscopy and Liquid Chromatography-Mass Spectrometry (LC-MS) (Fig. 3 – supplement 1).

Cells were pulse labelled with DAAs (D-amino acids) from <15 s to 5 minutes. Even at the very shortest labelling time (<15 s) peptidoglycan synthesis was observed both at the septum and cell periphery but without discrete foci (Fig. 3 – supplement 2a, b). Localisation microscopy of 15 s ADA and ADA-DA labelled cells revealed labelling occurs dispersed across the whole septum as well as the off-septal cell wall (Fig. 3a, Fig. 3 – supplement 2d). This was not due to non-specific labelling (Fig. 3 – supplement 2c). XY localisation precision (estimated by the Nikon NSTORM software) was 9.9 (s.d. 3.5) nm or 7.5 nm by NeNA (19). A similar pattern of peptidoglycan synthesis was seen with up to 5 min labelling with ADA or ADA-DA as a zone across the developing septum as well as throughout the off-septal cell wall (Fig. 3b, c, d). Previously PBP4 has been implicated in the presence of off-septal incorporation (3, 28), we therefore carried out DAA labelling and localisation microscopy in a PBP4 null background (SH4425) (Fig. 3 – supplement 3). Cell growth and GlcNAc incorporation were found to be the same as WT, however DAA labelling was reduced in SH4425 (Fig. 3 – supplement 3b-d). The proportion of off-septal labelling was

calculated in both SH1000 and SH4425 when labelled with ADA-DA, however no significant difference was observed (Fig. 3 – supplement 3e). Localisation microscopy of both 15s and 5 min labelled SH4425 showed peptidoglycan synthesis both at the septal and peripheral cell wall. Discrete foci of insertion were not observed (Fig. 3 – supplement 3f-g). Comparison of autocorrelations (as calculated for EzrA and FtsZ, using elliptical fits) for SH1000 and SH4425 revealed no substantial differences (Fig. 3 supplement 3h).

In cells with an incomplete septum, there was a "gap" in peptidoglycan synthesis at the mother cell wall-septum interface (Fig. 3c-i, arrows). In order to investigate the properties of the observed "gap" we used a counter stain to determine if it is filled with peptidoglycan. Fluorescent vancomycin has been used extensively to label peptidoglycan (29). Thus, we synthesised a version of this molecule with a Cy3B fluorophore so it could be used in two colour localisation microscopy with Alexa Fluor 647 click tagged amino acids. Vancomycin binds D-alanyl-D-alanine motifs in peptidoglycan and as these are highly prevalent in *S. aureus* the majority of peptidoglycan is fluorescently labelled. Our two colour images show that the "gap" regions that do not contain ADA-DA (5 minutes labelling), are nonetheless bound by vancomycin and thus are filled with peptidoglycan (Fig. 3e).

Also, cells with a filled septal annulus showed continued insertion that could be resolved into 2 distinct zones, one for each daughter (Fig. 3c-ii). These features were not observable by SIM, being smaller than its theoretical resolution.

Inhibition of cell division leads to co-mislocalization of the cell division components and peptidoglycan synthesis

The FtsZ inhibitor PC190723 prevents depolymerisation of FtsZ and consequently inhibits cell division, also leading to swollen *S. aureus* cells (30). It has previously been shown by diffraction limited fluorescence microscopy that PC190723 causes mislocalisations of FtsZ and PBP2 (31). We sought to determine the dynamics of this process, and the molecular pattern of associated peptidoglycan insertion. PC190723 treatment led to delocalization of peptidoglycan biosynthesis, EzrA and FtsZ even before substantial cell swelling (Figure 4 – supplement 1). Incorporation of HADA does not cause mislocalisation of FtsZ or EzrA (data not shown). Peptidoglycan synthesis was observed around the cell periphery and in distinct foci in the same place as EzrA and FtsZ. This non-uniform peptidoglycan insertion results in misshapen cells with irregular thickening of the cell wall (Fig. 4a). After 60 min treatment, patches of FtsZ, EzrA and peptidoglycan synthesis can be seen (Figure 4 – supplement 1a). Localisation microscopy of

peptidoglycan synthesis shows cell shape and the off-septal synthesis with patches of increased synthesis more clearly (Fig. 4b). Thus peptidoglycan synthesis follows localization of FtsZ and EzrA.

Morphology of the *Staphylococcus aureus* septum

It has been shown that the incomplete *S. aureus* septum is thinner at the leading than at the lagging edge (32, 33). However, the significance of this has remained unknown. We observed sections of cells from different stages in the cell cycle and measured septal geometry using thin section Transmission Electron Microscopy (TEM). The septum of *S. aureus* is thinner at the leading edge and progressively thicker towards the lagging edge until it fuses, at which point it is thinner at the centre and progressively thicker towards the lagging edge until ultimately uniform thickness is established (Fig. 5a, b). This dictates that peptidoglycan insertion cannot be confined to the leading edge of the septum and gives a morphological explanation for the observed peptidoglycan insertion pattern.

The surface area available for peptidoglycan insertion in the nascent septum was modelled resulting in the following expression for septal surface area prior to fusion (Fig. 5c):

$$A = \pi(2r - s)\sqrt{s^2 + d^2}$$

Where *d* is half the thickness of the septum, *r* is the radius of the cell in the plane of septation and *s* is the distance from the leading to the lagging edge of the septum (measured from the inner surface of the cell wall).

The surface area of a septum with consistently uniform thickness is that of the leading edge of that septum:

$$A = 4\pi(r - s)d$$

Not only is the available surface area always larger for the morphology we observe, but it increases as the septum closes (whereas with a uniformly thick septum, it decreases). This provides a framework for septal synthesis in an organism in which the septum comprises a substantial proportion of the cell wall.

Discussion

The non-standard cross section of the septum in *S. aureus* distinguishes it from other model organisms (Fig. 5a, b, c) and indicates that not all peptidoglycan insertion occurs at the leading edge of the septum in this species prompting the development of a new model for how peptidoglycan is synthesised during the cell cycle (Fig. 5d). This is likely advantageous to the bacteria, enabling more biosynthetic enzymes to work on the cell wall without steric hindrance. We sought to explain this phenomenon by analysing the distribution of peptidoglycan insertion and investigating key cell division components. Our novel application

of localisation microscopy to DAAs revealed that even at the shortest timescales and with considerably more precision than previous studies (3, 4, 34), there were no foci of peptidoglycan insertion – the diffuse pattern throughout the septum and periphery of the cell was ever-present. This surprising finding was corroborated by the distribution of core cell division components in *S. aureus*. Localisation microscopy of FtsZ and EzrA in the septal ring showed, like the distribution of peptidoglycan insertion, that they occurred in a zone, and were not limited to the leading edge of the septum. Also, FtsZ remained at the septum after the annulus had fused. When FtsZ depolymerisation was inhibited, peptidoglycan insertion was found to occur in areas with large amounts of FtsZ, resulting in local thickening of the cell wall, suggesting all synthesis may depend on FtsZ. This is a different scenario to *E. coli* and *B. subtilis*, where division-associated foci of peptidoglycan synthesis have been identified (albeit without the precision of localisation microscopy) and associated with cell division components driven by treadmilling FtsZ filaments (6, 7).

The divisome has been proposed to be a multi-component machine, present within a ring, based on diffraction-limited microscopy and interaction studies (10, 35). Previous localisation microscopy studies have begun to reveal intricate structural and spatial relationships between division components (36-38). Our data shows that divisome components are not placed exclusively at the leading edge of the septum, and that some individual proteins move more rapidly than others. There may, therefore, be a number of essentially identical machines executing peptidoglycan insertion within a region of the septum, with exchange of machine components with a more mobile population of molecules. It could also be the case that the machines are very non-uniform and can execute their tasks with a subset of the complete list of divisome proteins and with more or less of an individual protein. Alternatively, stable, stoichiometric complexes are not present and the interactions between proteins required to make new peptidoglycan are highly transient.

Materials and Methods

Bacterial Growth Conditions

Strains used in this study are listed in Appendix I Table 1, while plasmids and oligonucleotide sequences are shown in Appendix I Table 2 and Appendix I Table 3. *S. aureus* was grown in Brain Heart Infusion (BHI) broth at 37°C with aeration at 250 rpm, except for Slimfield microscopy and ^{14}C-GlcNAc incorporation experiments (and associated growth curves) which were carried out using Chemically Defined Media (CDM) (39). For solid media 1.5% (w/v) agar was added. Where required, antibiotics were added at the following concentrations; erythromycin (5 μg ml^{-1}), lincomycin (25 μg ml^{-1}), kanamycin (50 μg ml^{-1}), and

tetracycline (5 µg ml^{-1}). To induce protein production strains carrying gene fusions under the control of the Pspac promoter were grown in the presence of 50 µM isopropyl β-D-thiogalactopyranoside (IPTG).

Construction of *S. aureus* mutants

All vectors were constructed in *E. coli* NEB5α (New England Biolabs) following previously described methods (40, 41). The resulting constructs were passed through a restriction-deficient *S. aureus* RN4220 before being transduced into a final *S. aureus* SH1000 strain. Transformation and phage transduction of *S. aureus* were carried out as described previously (42, 43).

SH4388 (*ezrA-eyfp ΔezrA*): The EzrA-eYFP fusion was created by EcoRI and BamHI digestion of pGM074 and insertion of *eyfp* amplified by PCR from SU492(44) using primer pair eYFP-F and eYFP-R. pGM074 is pKASBAR-kan(35) containing *ezrA* under the control of its own promoter with the C-terminal *psmorange* (flanked by AscI and NotI restriction sites). In the resulting plasmid pKASBAR-EzrA-eYFP the translational fusion of *ezrA-eyfp* is linked by linker A (see below). pKASBAR-EzrA-eYFP was electroporated into CYL316(45) and its integration at the *geh* locus was confirmed by disruption of lipase production on Baird-Parker medium. The chromosomal fragment containing the integrated plasmid was moved into *S. aureus* SH1000 by phage transduction, creating SH4384 (*ezrA-eyfp*).

To delete native *ezrA,* an *ezrA* deletion vector was constructed. Fragments encompassing ~1.5 kb regions flanking *ezrA* were PCR amplified from *S. aureus* SH1000 genomic DNA using pOB-ezrA-up-F/-R and pOB-ezrA-down-F/-R. A 2.1 kb fragment encoding a tetracycline resistance cassette (TetR) was amplified from pAISH by PCR using pOB-TetR-F/-R primers. The three PCR products were ligated with HindIII and EcoRI cut pOB(46) by Gibson assembly, creating a deletion vector pOB-*ΔezrA*. The plasmid pOB-*ΔezrA* was electroporated into RN4220. The plasmid integrated into the chromosome through a single cross-over event and the DNA fragment containing the deletion cassette was transduced into SH4386 (*ezrA-eyfp*). Tetracycline-resistant/erythromycin-sensitive colonies were selected. In the resulting strain, SH4388 (*ezrA-eyfp ΔezrA*), *ezrA-eyfp* was the only copy of the *ezrA* gene. Replacement of *ezrA* for TetR was confirmed by PCR and Southern blot.

SH4640 (*ezrA-gfp ΔezrA*): To construct an EzrA-GFP translational fusion linked by linker A, *gfp* was PCR amplified from JGL227(10) using GFP-F/-R primers and ligated into AscI and EcoRI cut pGM074, creating pKASBAR-EzrA-GFP. The resulting plasmid was electroporated into CYL316. pKASBAR-EzrA-GFP integration at the *geh* locus was confirmed by disruption of lipase production on Baird-Parker medium. The chromosomal region containing the plasmid integrated within *geh* was moved to SH1000 creating SH4639

(*ezrA-gfp*). To delete native *ezrA*, SH4639 was transduced with a phage lysate from SH4388 (*ezrA-eyfp ΔezrA*), creating SH4640 (*ezrA-gfp ΔezrA*). Replacement of *ezrA* for TetR was confirmed by PCR and Southern blot.

SH4642 (*ezrA-snap ΔezrA*): A translational fusion of EzrA linked by linker A to the SNAP tag was constructed by PCR amplification of *snap* from pSNAP-tag (T7)-2 (New England Biolabs) using SNAP-F/-R primers. The PCR product was ligated into pGM074 using AscI and EcoRI cut sites to create pKASBAR-EzrA-SNAP. The resulting plasmid was electroporated into CYL316 and its integration at the *geh* locus was confirmed by disruption of lipase production on Baird-Parker medium. The chromosomal fragment containing integrated pKASBAR-EzrA-SNAP was transduced into SH1000, resulting in SH4641 (*ezrA-snap*). Native *ezrA* was replaced by TetR by transducing SH4641 with the phage lysate from SH4388 (*ezrA-eyfp ΔezrA*), creating SH4642 (*ezrA-snap ΔezrA*). Replacement of *ezrA* for TetR was confirmed by PCR and Southern blot.

SH4604 (*ezrA-meyfp ΔezrA*): To create a C-terminal fusion of EzrA with monomeric eYFP (meYFP) the whole pKASBAR-EzrA-eYFP plasmid was PCR amplified using meYFP-F/-R primers. The meYFP-F primer introduced an A207K substitution(47) into the *eyfp* gene. The PCR product was digested with DpnI to remove methylated DNA, the 5' ends of DNA were phosphorylated with T4 polynucleotide kinase (New England Biolabs) and DNA was circularized using Quick-Stick ligase (Bioline), resulting in pKASBAR-EzrA-meYFP. The resulting plasmid was electroporated into CYL316. The chromosomal fragment containing the integrated plasmid in the *geh* locus was moved into *S. aureus* SH1000 by phage transduction, creating SH4603 (*ezrA-meyfp*), To delete native *ezrA*, SH4603 was transduced with a phage lysate from SH4388 (*ezrA-eyfp ΔezrA*), creating SH4604 (*ezrA-meyfp ΔezrA*). Replacement of *ezrA* for TetR was confirmed by PCR and Southern blot.

SH4652 (*ezrA-eyfp ΔezrA* pCQ11-FtsZ-SNAP): In order to construct a strain simultaneously producing EzrA-eYFP and FtsZ-SNAP, a plasmid encoding a translational *ftsZ-snap* fusion placed under the control of the Pspac promoter was constructed. The *ftsZ* gene was PCR amplified from *S. aureus* N315 genomic DNA using FGFtsZXhoI-F and FGFtsZEcoRI-R primers and cloned into EcoRI and XhoI cut pSS26b (Covalys), resulting in pSS26bFtsZ-C. The fragment encoding *ftsZ-snap* was PCR amplified from pSS26bFtsZ-C using FGFtsZNheI-F and FGFtsZAscI-R and inserted into pCQ11(48) using NheI and AscI cut sites, creating pCQ11-FtsZ-SNAP. The plasmid was electroporated into RN4220 and moved to

SH4388 (*ezrA-eyfp ΔezrA*) by phage transduction, resulting in SH4652 (*ezrA-eyfp ΔezrA* pCQ11-FtsZ-SNAP).

SH4665 (pCQ11-FtsZ-eYFP): To construct a translational fusion of FtsZ with eYFP, an insert containing a fragment of linker B (see below) followed by a full length *eyfp* gene was synthesized by the GeneArt Gene Synthesis service, PCR amplified using ftsZ-eyfp-F/-R primers and cloned into NcoI and AscI cut pCQ11-FtsZ-SNAP, creating pCQ11-FtsZ-eYFP. The plasmid was electroporated to RN4220 and moved to SH1000 by phage transduction, resulting in SH4665 (pCQ11-FtsZ-eYFP).

SH4425 (*pbp4*): NE679 (*pbp4*) containing a transposon insertion within the *pbp4* gene was obtained from NARSA library (49). SH1000 was transduced with a phage lysate from NE679. Insertion of the transposon within *pbp4* in resulting SH4425 (*pbp4*) was confirmed by PCR and sequencing.

Sequences of genes encoding fluorescent proteins, tags and linkers

eyfp in pKASBAR-EzrA-eYFP, pMAD-eYFP-PBP2, pCQ11-eYFP-PBP2

ATGGTGAGCAAGGGCGAGGAGCTGTTCACCGGGGTGGTGCCCATCCTGGTCGAGCTGGACGGCG
ACGTAAACGGCCACAAGTTCAGCGTGTCCGGCGAGGGCGAGGGCGATGCCACCTACGGCAAGCT
GACCCTGAAGTTCATCTGCACCACCGGCAAGCTGCCCGTGCCCTGGCCCACCCTCGTGACCACCT
TCGGCTACGGCCTGCAGTGCTTCGCCCGCTACCCCGACCACATGAAGCAGCACGACTTCTTCAAGT
CCGCCATGCCCGAAGGCTACGTCCAGGAGCGCACCATCTTCTTCAAGGACGACGGCAACTACAAG
ACCCGCGCCGAGGTGAAGTTCGAGGGCGACACCCTGGTGAACCGCATCGAGCTGAAGGGCATCG
ACTTCAAGGAGGACGGCAACATCCTGGGGCACAAGCTGGAGTACAACTACAACAGCCACAACGTCT
ATATCATGGCCGACAAGCAGAAGAACGGCATCAAGGTGAACTTCAAGATCCGCCACAACATCGAGG
GCGGCAGCGTGCAGCTCGCCGACCACTACCAGCAGAACACCCCCATCGGCGACGGCCCCGTGCT
GCTGCCCGACAACCACTACCTGAGCTACCAGTCCGCCCTGAGCAAAGACCCCAACGAGAAGCGCG
ATCACATGGTCCTGCTGGAGTTCGTGACCGCCGCCGGGATCACTCTCGGCATGGACGAGCTGTAC
AAG

eyfp in pCQ11-FtsZ-eYFP

ATGGTTTCAAAAGGTGAAGAATTATTCACAGGTGTTGTTCCAATTTTGGTTGAATTAGATGGTGATGT
TAATGGTCATAAATTCTCAGTTTCAGGTGAAGGTGAAGGTGATGCAACATATGGTAAATTAACATTAA
AATTTATTTGTACAACAGGTAAATTACCAGTTCCTTGGCCAACATTAGTTACAACATTCGGTTATGGT
TTACAATGTTTTGCACGTTATCCAGATCATATGAAACAACATGATTTTTTCAAATCAGCAATGCCTGA
AGGTTATGTTCAAGAACGTACAATTTTCTTTAAAGATGATGGTAATTACAAAACACGTGCTGAAGTGA
AATTTGAAGGTGATACATTAGTTAATCGTATTGAATTAAAAGGTATTGATTTTAAAGAAGATGGAAATA
TTTTAGGTCATAAATTAGAATATAATTATAATTCACATAATGTTTATATTATGGCAGATAAACAAAAAAA
TGGTATTAAAGTTAATTTCAAAATTCGTCATAATATTGAAGGTGGTTCAGTTCAATTAGCAGATCATTA
TCAACAAAATACACCTATTGGTGATGGTCCAGTTTTATTACCAGATAATCATTATTTATCATATCAATC
AGCATTATCAAAAGATCCAAATGAAAAACGTGATCATATGGTTTTATTAGAATTTGTTACAGCAGCAG
GTATTACATTAGGTATGGATGAATTATATAAATAA

gfp in pKASBAR-EzrA-GFP

ATGGCTAGCAAAGGAGAAGAACTTTTCACTGGAGTTGTCCCAATTCTTGTTGAATTAGATGGTGATG
TTAATGGGCACAAATTTTCTGTCAGTGGAGAGGGTGAAGGTGATGCTACATACGGAAAGCTTACCC
TTAAATTTATTTGCACTACTGGAAAACTACCTGTTCCATGGCCAACACTTGTCACTACTTTGACCTAT
GGTGTTCAATGCTTTTCCCGTTATCCGGATCATATGAAACGGCATGACTTTTTCAAGAGTGCCATGC
CCGAAGGTTATGTACAGGAACGCACTATATCTTTCAAAGATGACGGGAACTACAAGACGCGTGCTG

AAGTCAAGTTTGAAGGTGATACCCTTGTTAATCGTATCGAGTTAAAAGGTATTGATTTTAAAGAAGAT
GGAAACATTCTCGGACACAAACTCGAGTACAACTATAACTCACACAATGTATACATCACGGCAGACA
AACAAAAGAATGGAATCAAAGCTAACTTCAAAATTCGCCACAACATTGAAGATGGATCCGTTCAACT
AGCAGACCATTATCAACAAAATACTCCAATTGGCGATGGCCCTGTCCTTTTACCAGACAACCATTAC
CTGTCGACACAATCTGCCCTTTCGAAAGATCCCAACGAAAAGCGTGACCACATGGTCCTTCTTGAGT
TTGTAACTGCTGCTGGGATTACACATGGCATGGATGAGCTCTACAAATAA

snap in pSNAP-tag (T7)-2 and pKASBAR-EzrA-SNAP

ATGGACAAAGACTGCGAAATGAAGCGCACCACCCTGGATAGCCCTCTGGGCAAGCTGGAACTGTC
TGGGTGCGAACAGGGCCTGCACCGTATCATCTTCCTGGGCAAAGGAACATCTGCCGCCGACGCCG
TGGAAGTGCCTGCCCCAGCCGCCGTGCTGGGCGGACCAGAGCCACTGATGCAGGCCACCGCCTG
GCTCAACGCCTACTTTCACCAGCCTGAGGCCATCGAGGAGTTCCCTGTGCCAGCCCTGCACCACC
CAGTGTTCCAGCAGGAGAGCTTTACCCGCCAGGTGCTGTGGAAACTGCTGAAAGTGGTGAAGTTC
GGAGAGGTCATCAGCTACAGCCACCTGGCCGCCCTGGCCGGCAATCCCGCCGCCACCGCCGCCG
TGAAAACCGCCCTGAGCGGAAATCCCGTGCCCATTCTGATCCCCTGCCACCGGGTGGTGCAGGGC
GACCTGGACGTGGGGGGCTACGAGGGCGGGCTCGCCGTGAAAGAGTGGCTGCTGGCCCACGAG
GGCCACAGACTGGGCAAGCCTGGGCTGGGT

snap in pSS26b, pSS26bFtsZ-C and pCQ11-FtsZ-SNAP

ATGGACAAAGATTGCGAAATGAAACGTACCACCCTGGATAGCCCGCTGGGCAAACTGGAACTGAGC
GGCTGCGAACAGGGCCTGCATGAAATTAAACTGCTGGGTAAAGGCACCAGCGCGGCCGATGCGGT
TGAAGTTCCGGCCCCGGCCGCCGTGCTGGGTGGTCCGGAACCGCTGATGCAGGCGACCGCGTGG
CTGAACGCGTATTTTCATCAGCCGGAAGCGATTGAAGAATTTCCGGTTCCGGCGCTGCATCATCCG
GTGTTTCAGCAGGAGAGCTTTACCCGTCAGGTGCTGTGGAAACTGCTGAAAGTGGTTAAATTTGGC
GAAGTGATTAGCTATCAGCAGCTGGCGGCCCTGGCGGGTAATCCGGCGGCCACCGCCGCCGTTAA
AACCGCGCTGAGCGGTAACCCGGTGCCGATTCTGATTCCGTGCCATCGTGTGGTTAGCTCTAGCG
GTGCGGTTGGCGGTTATGAAGGTGGTCTGGCGGTGAAAGAGTGGCTGCTGGCCCATGAAGGTCAT
CGTCTGGGTAAACCGGGTCTGGGATGA

Linker A

TCAGGTTCAGGTTCAGGTGGGCGCGCCTCAGGTTCAGGTTCAGGT

Linker B

GAATTCCCCATGGGTTCAGGTGGTGGTGGTTCA

Labelling *S. aureus* with DAAs

DAAs were prepared by published methods (9-11) or by modified procedures described in Appendix II. ADA was obtained from Iris Biotech. These were incubated with mid-exponential phase (OD_{600} ~ 0.3 to 0.4) *S. aureus* at 500 µM (1 mM for ADA-DA) and incubated on a rotary shaker at 37°C for the required labelling time. Samples were imaged using widefield microscopy, 3D-SIM or localisation microscopy as required. For 15 s labelling DAAs were used at 10 mM, 1ml samples were mixed briefly by vortexing and fixed by addition of 500 µl 8% (w/v) ice-cold paraformaldehyde immediately after vortexing.

Click Chemistry

DAAs containing an azide functional group (ADA & ADA-DA) required chemical attachment of a fluorophore via the Click reaction (copper (I)-catalysed alkyne-azide cycloaddition). This was carried out using the Click-iT® Cell Reaction Buffer Kit (ThermoFisher) as per the manufacturers protocol. Alkyne dyes were added at 5 µg ml^{-1}.

Labelling *S. aureus* with Fluorescent Vancomycin

Fixed cells were resuspended in PBS containing fluorescent vancomycin at 2 µM (prepared using succinimidyl ester of Amersham Cy3B (GE Healthcare) as previously described(29). Samples were protected from light and incubated at room temperature for 30 minutes then washed by centrifugation and resuspension in water. For dual labelled samples, cells were labelled with required DAA as described above and fixed with 4% (w/v) paraformaldehyde prior to labelling with fluorescent vancomycin.

Labelling *S. aureus* with NHS ester

S. aureus grown to mid-exponential phase (OD_{600} ~0.5) were resuspended in PBS containing Alexa Fluor 647 NHS ester (Invitrogen) at 8 µg ml^{-1} and incubated at room temperature for 5 min. Cells were then washed by centrifugation and resuspension in PBS.

Labelling *S. aureus* with SNAP-Cell TMR-Star

S. aureus grown to mid-exponential phase (OD_{600} ~0.5) were incubated with SNAP-Cell TMR-Star (New England Biolabs) at 500 nM for widefield microscopy or 3 µM for SIM at 37°C for 15 min. Cells were washed by centrifugation and resuspension in PBS.

Fixing

With the exception of Slimfield microscopy which involved no fixation and 15 s DAA labelling which used 8% (w/v) ice-cold paraformaldehyde, all samples were fixed with 4% (w/v) paraformaldehyde prior to imaging.

Widefield Epifluorescence Microscopy

Fixed cells were mounted on poly-L-Lysine coated slides and imaged on a Nikon Ti Inverted microscope fitted with a Lumencor Spectra X light engine. Images were taken using a 100x PlanApo (1.4 NA) oil objective using 1.518 RI oil and detected by an Andor Zyla sCMOS camera.

OMX Microscopy

Coverslips (High-precision, No.1.5H, 22x22mm, 170±5 µm, Marienfeld) were sonicated for 15 min in 1 M KOH, washed with water and incubated in poly-L-Lysine solution for 30 minutes. Coverslips were then further washed and dried with nitrogen. Fixed cells were then dried onto the coverslips with nitrogen and mounted on slides with ~5 µl Slow Fade Diamond (Invitrogen).

Structured Illumination Microscopy was carried out using a v4 DeltaVision OMX 3D-SIM system fitted with a Blaze module (Applied Precision, GE Healthcare, Issaquah, USA). Samples were illuminated using laser

illumination. For each z slice, samples were imaged in 5 phase shifts and 3 angles, z-steps were 0.125 nm. Reconstructions were performed with the Softworx software (GE Healthcare) using OTFs optimised for the specific wavelength and oil used. The same software was used for deconvolution.

Sample Preparation for Localisation Microscopy

For all samples coverslips were prepared as for 3D-SIM Microscopy. All samples except for eYFP/meYFP and were mounted on slides with 5 µl GLOX buffer (0.5 mg ml^{-1} glucose oxidase, 40 µg ml^{-1} catalase, 10% (w/v) glucose in 50 mM Tris-HCl containing 10 mM NaCl (pH 8.0) containing either 10 or 100 mM mercaptoethylamine (MEA).

For eYFP/meYFP imaging (single colour) samples were mounted in 5 µl PLOX buffer (5 U ml^{-1} pyranose oxidase, 40 µg ml^{-1} catalase, 10% (w/v) glucose in 50 mM Tris-HCl, 10 mM NaCl (pH 8.0) prepared in heavy water(50)).

For eYFP/Alexa Fluor 647 imaging (two-colour) samples were mounted in 5 µl PLOX containing 50 mM MEA. Where required, coverslips were sparsely coated with TetraSpeck beads (0.1 µm, Molecular Probes) prior to the application of cells.

Bespoke Localisation Microscope

Localisation microscopy was carried out as previously described(51, 52), but using OBIS 405 (50 mW) and OBIS 647 (120 mW) lasers, a 662 nm dichroic and a 676 (29) nm emission filter. Calibration data for 3D reconstructions was obtained by recording images of fiducial particles while stepping the objective piezo.

Nikon N-STORM Localisation Microscope

Localisation microscopy was carried out using a Nikon Ti-NS N-STORM version 1 with 3D capability in continuous mode. Objective used was a SR Apo TIRF 100x NA 1.49 and images detected using EMCCD camera (Andor DU-897) using the 17 MHz 16 bit mode with an EM Multiplier Gain of 300 and a conversion gain of 3. Calibration data for 3D reconstructions was obtained by recording images of fiducial particles using the calibration mode. Custom-made filter cubes were used for eYFP/meYFP (no excitation filter, 488 nm dichroic, 525/50 nm emission) and two-colour imaging (red/far red; no excitation filter, multi-band dichroic with transmission at 410-480 nm, 500-550 nm, 570-630 nm and above 650 nm, multi-band emission with transmission at 570-620 nm and above 660 nm) imaging and the N-STORM cube for single colour Alexa Fluor 647 imaging. Imaging was done under oblique illumination but not full TIRF. Two colour

eYFP and Alexa Fluor 647 imaging was performed using separate filter cubes whereas two colour imaging using Cy3B and Alexa Fluor 647 was performed using a single cube, as specified.

Image Reconstruction

Images were reconstructed as previously described(53) using either custom Matlab scripts, the ThunderSTORM ImageJ/Fiji plugin(54) or Nikon elements software. All of these methods identify the locations of molecules by fitting Gaussian functions to regions of source data, and all yielded similar results.

Two colour data (where using a single multi-band filter cube) was reconstructed and aligned (registered) using Nikon elements. In summary, alignment is achieved by obtaining calibration images of the same fluorescent beads in both channels. The software then determines the way in which localisations in one channel must be offset to align with the other, based on the offsets in the apparent positions of the beads. For two colour eYFP/Alexa Fluor 647 NHS ester imaging, using two filter cubes, the average position of a TetraSpeck fiducial was determined in both channels and a translational offset calculated for each image. This was applied to the Alexa Fluor 647 channel to approximately align the data. Whilst more sophisticated co-alignment methods exist, this was sufficient for us to draw the qualitative conclusions necessary for this part of our study.

Image Rendering

Images were rendered as 2D histograms using the ThunderSTORM ImageJ/Fiji plugin(54). Unless otherwise stated images were projected onto a single plane and the reconstructed pixel size was 10 nm. Semi-quantitative Matlab contour plots were used in some instances for ease of visualisation of key features in 3D reconstructions both on screen and in print. eYFP and eYFP/Alexa Fluor 647 NHS ester dual colour images were reconstructed with a pixel size of 5 nm with a Gaussian blur of 20 nm applied to make them easier to see.

Analysis of Localisation Microscopy Data

Ring-like groups of localisations were manually selected from fields. The centre and radius of a circle that best fit the points was then determined allowing the localisations to be represented using polar co-ordinates. Histograms of localisations with respect to angle (2˚ bin size) and distance from the centre of the circle (10 nm bin size) were then generated. The angular histograms were auto-correlated to test for the presence of similarly sized large groups of molecules which would create peaks or a very slow decay

from 0˚ in the resulting graph. The distance histograms were plotted and compared with those resulting from simulations.

An additional, similar, analysis was carried modelling the septal shape as an ellipse (Fig. 1 - supplement 3).

Simulation of Localisation Microscopy Data

We used the simplest possible methods to simulate data to compare with that acquired on the microscope. Localisations were randomly distributed by angle on circles of a fixed radius. Localisation error comes from several physical sources, but was simulated by adding offsets in x and y taken independently and at random from a normal distribution of a defined standard deviation.

Slimfield Microscopy: Microscope Setup

A bespoke single-molecule microscope was used, constructed around the body of a Zeiss inverted microscope with a 100x 1.49 numerical aperture oil immersion total internal reflection fluorescence (TIRF) objective lens (Olympus) and an xyz nano positioning stage (Nanodrive, Mad City Labs). A 20 mW Obis 514 nm laser expanded to 10 µm full width at half maximum was used to excite meYFP fluorescence combined with a dual pass CFP/YFP dichroic mirror with 20 nm transmission windows centred on 440 nm and 514 nm. A high speed camera (Andor iXon DV860-BI) was used to image at 5 ms/frame with magnification at 50 nm/pixel. Data was acquired using custom LabView software.

Slimfield Microscopy: Sample preparation and imaging

S. aureus SH4604 (*ezrA-meyfp ΔezrA*) cells were imaged by immobilising them on an agarose pad suffused with media. These were constructed by placing a gene frame (Life Technologies) on a BK7 glass microscope slide (Fisher) and filling with ~500 µl 1% (w/v) agarose containing media. Once set, 5 µl of cell culture was spotted over the agarose and covered with a plasma cleaned coverslip.

Slimfield Microscopy: Image analysis

Cell bodies and apparent EzrA rings were segmented as outlined previously(55). In brief, the cell body was found by segmenting both a 5 frame average EzrA-meYFP fluorescence and brightfield image using a threshold set by the background peak in the pixel intensity distribution. The brightfield segmentation was used as seeds for watershedding the segmented fluorescence image to identify individual cells. Further thresholding within cell pixels yields a mask for the EzrA ring.

Diffraction-limited fluorescent foci were tracked using custom Matlab software as described previously(56). In brief, in each frame, candidate foci are identified by thresholding top-hat transformed images using

Otsu's method. The spot centre is determined to sub-pixel precision using iterative Gaussian masking(57) and accepted if its signal-to-noise ratio, as defined by the foci intensity, the background-corrected integrated pixel intensity within a 5 pixel radius circular region of interest centred of the foci intensity centroid, divided by the standard deviation of the background pixels, is greater than 0.4. Foci are linked into the same track between image frames if they are within a distance of 1 optical resolution width (approximately 5 pixels), generating single particle tracks to a typical localization precision of ~40 nm(58). The mean squared displacement of each track over its first 4 time interval points was used to calculate its microdiffusion coefficient, D, using a linear fit(59). These were binned into 0.01 $\mu m^2\ s^{-1}$ bins and fitted with 1-3 gamma functions(26), with 3 gammas generating the lowest reduced chi^2.

Copy number values were calculated using a deconvolution method called CoPro(27) which utilised the symmetrical geometry of *S. aureus* cells and the *in vivo* characteristic intensity of single meYFP molecules(60). Detection of single meYFP was confirmed by observation of single, distinct photobleach steps. This characteristic brightness value corresponding to a single meYFP molecule was determined as the peak of the intensity distribution of fluorescent foci found after 200 ms of photobleaching, and was equivalent to 2000±500 counts on our EMCCD camera detector.

Transmission Electron Microscopy

Samples were prepared for electron microscopy as previously described (35) .

Cell Volume Calculation

Cell volumes calculations were carried out as previously described(4), specifically, the long and short axis of cells were measured using Fiji. The volume was then calculated based on a prolate spheroid shape with volume $V = \frac{4}{3}\pi ab^2$, where a and b are the dimensions of the long and short axis respectively.

Gel-based analysis of SNAP tagged proteins

SNAP-Cell TMR-Star (New England Biolabs) was added to a 1 ml aliquot of mid-exponential phase (OD_{600} ~1) grown culture at a concentration of 500 nM and incubated at 37°C for 1 h. Cells were washed three times by resuspension and centrifugation in PBS, resuspended in PBS supplemented with 200 µg ml^{-1} lysostaphin and 20 U ml^{-1} DNase I and lysed at 37°C for 30 min. Cell extracts were resolved in SDS-PAGE, the gel was rinsed with dH_2O and scanned using ChemiDoc MP System (Bio-Rad).

Incorporation of ^{14}C-GlcNAc into cell wall Peptidoglycan

S. aureus strains were grown overnight in CDM and used to inoculate fresh CDM to an OD_{600} of 0.05 and grown to OD_{600} ~0.2. At this point 5 µM ^{14}C-GlcNAc was added to cultures. At 30 minute intervals samples

were collected and prepared for analysis of ^{14}C-GlcNAc incorporation via Liquid Scintillation as previously described(61).

Fluorescence Intensity Measurements

Fluorescence intensity was measured using Image J/Fiji and calculated as counts/pixel. To determine the % off-septal fluorescence the fluorescence intensity for both the septum and the whole cell was measured and the percentage of non-septal fluorescence calculated.

Peptidoglycan purification and Mass-Spectrometry Analysis

S. aureus peptidoglycan was purified as previously described(34). Specifically, 1L cultures of *S. aureus* SH1000 and *S. aureus* SH1000 containing 1 mM ADA were grown for 4 hours before peptidoglycan was extracted and purified. Peptidoglycan was solubilized by digestion with 50 µg Cellosyl per mg peptidoglycan (dry weight) overnight at 37°C. Samples were boiled to inactivate the Cellosyl and reduced using sodium borohydride(62). Reduced muropeptides were separated on an Agilent Technologies Accurate Mass Q-TOF LC/MS using a Hypersil Gold aQ column (200 x 42.1 µm, 1.9 µm particle size) with a gradient of 0-30 % (v/v) water/ACN both containing 0.1% (v/v) formic acid over 60 mins.

Acknowledgments

This work was funded by the Medical Research Council (MR/N002679/1, MR/K015753/1, G1100127, MR/K01580X/1) and the Biotechnology and Biological Science Research Council UK (BB/L006162/1, BB/N006453/1). We are grateful to Simon Thorpe, Chris Hill, Irene Johnson and Joe Kirk for their assistance.

Figure Legends

Figure 1. Distribution of cell division components during septation. a) Examples of EzrA distributions obtained using localisation microscopy of SH4388 (*ezrA-eyfp ΔezrA*). Scale bars 200 nm. b) Examples of FtsZ distributions obtained using localisation microscopy of SH4665 (pCQ11-FtsZ-eYFP) grown with 50µM IPTG. Scale bars 200 nm). c) Simulated distributions of localisations randomly distributed by angle with different radii (r), number of localisations (n) and random error from a normal distribution with standard deviation (σ) [i] r=440 nm, n=1118, σ=20 nm, [ii] r=440 nm, n=1118, σ=40 nm, [iii] r=440 nm, n=1118, σ=80 nm, [iv] r=440 nm, n=145, σ=20 nm, [v] r=440 nm, n=2010, σ=20 nm. Scale bars 200 nm. d) An enlarged example of EzrA-eYFP distribution. Scale bar 200 nm. e) The distribution from ‘d’ plotted as a scatter graph, and as histograms of number of localisations with respect to angle

and distance from centre. f) Mean angular autocorrelations of 14 EzrA, 19 FtsZ and 15 simulated distributions. Autocorrelation drops less quickly for EzrA and FtsZ than for simulations where angle is randomised. This shows that neither EzrA or FtsZ are randomly distributed by angle. g) Histograms of localisations with respect to distance from the centre of a fitted circle with varying localisation precision. Data for EzrA and FtsZ is spread more widely than simulated data with poor localisation precision.

Figure 2. Relative locations of division components. a) Localisation microscopy images: of FtsZ-eYFP distributions in bacteria in the late stages of division. Scale bars 500 nm. Ellipses show approximate cell location and orientation. b) Dual colour localisation microscopy image of FtsZ-eYFP and the cell wall (labelled with Alexa Fluor 647 NHS ester, NHS-647). Scale bars 500 nm. c) Dual colour localisation microscopy image of EzrA-eYFP and the cell wall (labelled with NHS-647). Scale bars 500 nm.

Figure 3. Peptidoglycan insertion. Localisation microscopy images: a) 15 s labelling of ADA (Azido-D-alanine) clicked to Alexa Fluor 647. Scale bars 0.5 µm. b) 5 min labelling of i) ADA clicked to Alexa Fluor 647 and ii) ADA-DA clicked to Alexa Fluor 647. Scale bars 1 µm. c) 3D projections of *S. aureus* labelled for 5 minutes with ADA clicked to Alexa Fluor 647. i) Cells with incomplete septum (yellow arrows show gaps in labelling), ii) cell with annulus complete. Images in black box are z-projections while 3D representations show projections in all 3 planes. Scale bar 0.5 µm. d) Cross sections of incomplete septa. The sketch graph (top row) hypothetically shows labelling exclusively at the leading edge of the septum. This is not the case for the data shown below - labelling is spread throughout the septum. The full width half maximum spread of labelling is ~230 nm. Data is plotted with blue dots, fits in red lines. e) Two colour STORM, sample labelled for 5 minutes with ADA-DA clicked to Alexa Fluor 647 (yellow) and vancomycin linked to Amersham Cy3B (magenta). Images are z-projections and in merged images where localisations are in white show labelling by both ADA-DA and vancomycin. Boxed regions show slot in ADA-DA labelling but not vancomycin. Scale bars 1 µm.

Figure 4. Effect of FtsZ inhibitor PC190723 on *S. aureus.* a) TEM of S. *aureus* SH1000 grown in the presence of PC190723 (10 µg ml^{-1}) for 60 minutes. Scale bars 200 nm. b) STORM image of *S. aureus* SH1000 pre-treated with PC190723 (10 µg ml^{-1}) for 60 minutes labelled with ADA clicked to Alexa Fluor

647 for 5 minutes. Scale bar 1 µm. i) & ii) zoomed images of the corresponding area, scale bars 0.25 µm.

Figure 5. Conceptual model of peptidoglycan insertion during the *S. aureus* cell cycle.

a) Schematic of measurement used in b) measurement of the angle (θ) between a line parallel to the surface of the septum (yellow) and a tangent to the surface of the bacterium in incomplete (blue) and complete (red) septa. c) Surfaces available for peptidoglycan insertion for different septal geometries where d is half the thickness of the septum, r is the cell radius in the septal plane and s is the distance from the leading to the lagging edge of the septum (measured from the inner surface of the cell wall). d) Conceptual model of peptidoglycan insertion in *S. aureus*. i, ii) Cell size increases and aspect ratio changes prior to observation of the start of septum formation by 3D-SIM (3). iii) The septum then starts to form, beginning with the "piecrust" feature (red) observed by AFM (34). The septum is thinner at the leading edge (33). iv) New peptidoglycan is inserted in a zone at the leading edge of the septum, as well as across the rest of the cell surface as visualised here by localisation microscopy. v, vi) After the annulus has fused, peptidoglycan insertion continues in the septum, executed by cell division components, until it is of uniform thickness. vii) ATL (a peptidoglycan hydrolase) is present at the outer surface of the cell in the plane of septation(63). Cracks or splits begin to form at the outer surface in the plane of septation(64), followed by rapid popping apart of the daughter cells (4). vii) "Scars" or "ribs" remain marking the site of division (3, 34) and may provide spatial cues to subsequently enable correct sequentially orthogonal divisions.

Supplementary Figure Legends

Figure 1 – figure supplement 1. EzrA fusions are functional. a) Construction of *S. aureus* strains in which the only copy of *ezrA* is tagged (FL). Integration of pKASBAR-EzrA-FL at *S. aureus* lipase (*geh*) resulted in an ectopic copy of *ezrA-fl* under the control of the native *ezrA* promoter (P). A double-crossover event of pOB-*ΔezrA* allowed for marked with a tetracycline resistance (tetR) gene deletion of *ezrA* from its native chromosomal location. FL represents either eYFP, meYFP, GFP or SNAP. Not to scale. b) Growth rates of *ezrA* fusions. EzrA-eYFP, EzrA-meYFP, EzrA-GFP and EzrA-SNAP complement native *ezrA* knock-out in SH4388 (*ezrA-eyfp ΔezrA*), SH4604 (*ezrA-meyfp ΔezrA*), SH4640 (*ezrA-gfp ΔezrA*) and SH4642 (*ezrA-snap ΔezrA*), respectively. The mutant strains (doubling time 24 min) showed similar growth to the wild type strain, SH1000 (doubling time 25 min). Growth rates were

obtained by fitting an exponential growth equation to the most linear region of growth curves (R^2 >0.98). Bacterial cultures were prepared in triplicate and the error bars represent standard deviation from the mean. c) Epifluorescence microscopy images of EzrA-eYFP in SH4388 (*ezrA-eyfp ΔezrA*), EzrA-meYFP in SH4604 (*ezrA-meyfp ΔezrA*), EzrA-GFP in SH4640 (*ezrA-gfp ΔezrA*) and SNAP-Cell TMR-Star labelled EzrA-SNAP in SH4642 (*ezrA-snap ΔezrA*). Images are maximum intensity fluorescence projections of z stacks. Scale bars 3 μm. d) EzrA-eYFP in SH4388 (*ezrA-eyfp ΔezrA*) and EzrA-meYFP in SH4604 (*ezrA-meyfp ΔezrA*) were detected by Western blot analysis of total protein extracts using anti-GFP antibodies. Whole cell lysate of SH1000 and a recombinant GFP-HisTag protein were used as controls. Bands detected at ~95 kDa (EzrA-eYFP and EzrA-meYFP) and ~28 kDa (GFP-HisTag) are indicated with black arrows. Sizes of a protein ladder are shown in kDa. e) EzrA-GFP in SH4640 (*ezrA-gfp ΔezrA*) was detected by immunoblot analysis of total protein extract using anti-GFP antibodies. Whole cell lysate of SH1000 and a recombinant GFP-HisTag protein were used as controls. Bands detected at ~95 kDa (EzrA-GFP) and ~28 kDa (GFP-HisTag) are indicated with black arrows. Sizes of a protein ladder are shown in kDa. f) Whole cell lysate of SNAP-Cell TMR-Star labelled SH4642 (*ezrA-snap ΔezrA*) was resolved by 10% (w/v) SDS-PAGE and visualised by fluorescence detection. Whole cell lysate of SNAP-Cell TMR-Star labelled SH1000 and a purified SNAP-Cell TMR-Star labelled HisTag-SNAP protein were used as controls. Bands detected at ~85 kDa (EzrA-SNAP) and ~23 kDa (SNAP-HisTag) are indicated with black arrows. Sizes of a protein ladder are shown in kDa.

Figure 1 – figure supplement 2. STORM and SIM data. a) EzrA-GFP (i) and SNAP-Cell TMR-Star labelled EzrA-SNAP (ii) localisation in SH4640 (*ezrA-gfp ΔezrA*) and SH4642 (*ezrA-snap ΔezrA*) by 3D-SIM, respectively. The images are maximum intensity projections of reconstructed z stacks. Scale bars 1 μm. 3D surface profiles of the circled area show distribution of fluorescence intensity of EzrA-GFP and EzrA-SNAP TMR-Star rings. b) Localisation microscopy of EzrA-meYFP in SH4604 (*ezrA-meyfp ΔezrA*).

Figure 1 – figure supplement 3. Quantitative analysis of EzrA and FtsZ distributions from localisation microscopy data based on elliptical fits. a) Example image of EzrA distribution. Scale bar 200 nm. b) EzrA distribution represented as a scatter plot overlaid on an elliptical ring. Yellow points are included in the subsequent analyses, grey ones are not. The elliptical ring is derived from an elliptical fit to all of the points. c) Enlargement of boxed region in b. The elliptical ring is split up into blocks – darker blue blocks contain more localisations than lighter ones. This gives a measure of how the number

of localisations varies around the ring. d) Autocorrelations of localisations around the ring for EzrA, FtsZ and simulated data with a random distribution. EzrA and FtsZ distributions are more self-correlated than a random distribution, but have no periodic order. e) Distributions of absolute distances of localisations from the fitted ellipse for EzrA, FtsZ and simulated data. Simulated data had a localisation precision from a normal distribution with a mean of 27 nm and a standard deviation of 8.7 nm – representative of our measured values. The spread and magnitude of distances of EzrA and FtsZ localisations from the fitted ellipse cannot be accounted for by localisation uncertainty alone.

Figure 2 – figure supplement 1. Dynamics of EzrA. Nominal diffusion coefficient (D) distributions of EzrA-meYFP molecules a) inside and b) outside the EzrA "ring" in SH4604 (*ezrA-meyfp ΔezrA*). The distribution of D values could be fitted using a 1-3 component gamma distribution model, as developed for heterogeneous protein mobility observed previously in bacteria (26), with 3 components producing the lowest reduced chi^2=0.05 c) Distribution of number of EzrA-meYFP molecules per cell.

Figure 3 – figure supplement 1. Identification of mechanism of DAA labelling in *S. aureus*. Cellosyl digested peptidoglycan from *S. aureus* SH1000 grown in the presence (a) or absence (b) of ADA for 4 hours were investigated using LC-MS, with total ion chromatogram for acquisition time 20-36 minutes showing all detected ions (i). ii) Extracted ion chromatogram for m/z $[H_+]$ = 1294.5970 shows a clear peak in (a) not present in (b). c) The mass-spectrum of this peak shows both the monoisotopic mass of the single-charged ion 1294.5863 and the doubly-charged ion at 647.7968, corresponding to disaccharide-pentapeptide-pentaglycine molecule with ADA replacing one of the D-alanine residues.

Figure 3 – figure supplement 2. 15 second labelling of peptidoglycan insertion with DAAs and controls. a) 15s labelling of ADA clicked to Alexa Fluor 647. Sample imaged by epifluorescence and image is a maximum intensity projection of z stacks. b) 15s labelling with HADA imaged by i) epifluorescence and ii) 3D-SIM. c) Cells labelled with Alexa Fluor 647 by the click reaction in the absence of ADA imaged by i) epifluorescence and ii) STORM. d) localisation microscopy of 15s labelling of ADA-DA (azido-D-alanyl-D-alanine) clicked to Alexa Fluor 647. Scale bars a-c) 5μm d) 1 μm.

Figure 3 – figure supplement 3. DAA labelling of PBP4 null *S. aureus*. a) SH4425 (SH1000 *pbp4*) labelled for 5 minutes with i) HADA and ii) ADA-DA clicked to Alexa Fluor 647. Scale bars 5 μm. b) Growth rate of SH1000 and SH4425 in CDM, c) Rate of peptidoglycan synthesis as measured by ^{14}C GlcNAc incorporation. d) DAA incorporation with 5 minutes labelling (HADA & ADA-DA) in SH1000 and SH4425. e) % off-septal labelling in 5 minutes ADA-DA labelling of SH1000 and SH4425. f) Localisation

microscopy of 5 minutes FDAA labelling of SH4425 with i) ADA clicked to Alexa Fluor 647 and ii) ADA-DA clicked to Alexa Fluor 647. Scale bars 1 µm. g) Localisation microscopy of 15s labelling of SH4425 with i) ADA clicked to Alexa Fluor 647 and ii) ADA-DA clicked to Alexa Fluor 647. Scale bars 1 µm. h) Comparison of autocorrelations of localisations around a fitted elliptical ring for SH1000 and SH4425 (SH1000 *pbp4*) labelled for 15 with i) ADA or ii) ADA-DA. n=10 bacteria per group. There is no substantial difference between autocorrelations in either comparison.

Figure 4 – figure supplement 1. Effect of FtsZ inhibitor PC190723 on *S. aureus*. a) SH4652 (*ezrA-eyfp ΔezrA* pCQ11-FtsZ-SNAP) grown in the presence of 50 µM IPTG in the absence (control) or presence of PC190723 (10 µg ml^{-1}) for 0, 15, 30 and 60 minutes, labelled with SNAP-Cell TMR-Star was incubated with HADA for 5 min. Images are average intensity projections of z stacks. Scale bars 3 µm. Arrows indicate localisation defects. b) Cell volume of *S. aureus* SH1000 during treatment with PC190723 (10 µg ml^{-1}). Data is expressed as mean ± standard deviation.

References

1. Turner RD, Vollmer W, Foster SJ. Different walls for rods and balls: the diversity of peptidoglycan. Mol Microbiol. 2014;91(5):862-74.
2. Cabeen MT, Jacobs-Wagner C. Bacterial cell shape. Nat Rev Microbiol. 2005;3(8):601-10.
3. Monteiro JM, Fernandes PB, Vaz F, Pereira AR, Tavares AC, Ferreira MT, et al. Cell shape dynamics during the staphylococcal cell cycle. Nature Communications. 2015;6:8055.
4. Zhou X, Halladin DK, Rojas ER, Koslover EF, Lee TK, Huang KC, et al. Bacterial division. Mechanical crack propagation drives millisecond daughter cell separation in *Staphylococcus aureus*. Science. 2015;348(6234):574-8.
5. Wheeler R, Turner RD, Bailey RG, Salamaga B, Mesnage S, Mohamad SA, et al. Bacterial Cell Enlargement Requires Control of Cell Wall Stiffness Mediated by Peptidoglycan Hydrolases. MBio. 2015;6(4):e00660.
6. Yang X, Lyu Z, Miguel A, McQuillen R, Huang KC, Xiao J. GTPase activity–coupled treadmilling of the bacterial tubulin FtsZ organizes septal cell wall synthesis. Science. 2017;355:744-7.
7. Bisson Filho AW, Hsu YP, Squyres GR, Kuru E, Wu F, Jukes C, et al. Treadmilling by FtsZ filaments drives peptidoglycan synthesis and bacterial cell division. Science. 2017;355:739-43.
8. Levin PA, Kurtser IG, Grossman AD. Identification and characterization of a negative regulator of FtsZ ring formation in Bacillus subtilis. Proc Natl Acad Sci U S A. 1999;96(17):9642-7.
9. Adams DW, Errington J. Bacterial cell division: assembly, maintenance and disassembly of the Z ring. Nat Rev Micro. 2009;7(9):642-53.
10. Steele VR, Bottomley AL, Garcia-Lara J, Kasturiarachchi J, Foster SJ. Multiple essential roles for EzrA in cell division of Staphylococcus aureus. Mol Microbiol. 2011;80(2):542-55.
11. Strauss MP, Liew AT, Turnbull L, Whitchurch CB, Monahan LG, Harry EJ. 3D-SIM super resolution microscopy reveals a bead-like arrangement for FtsZ and the division machinery: implications for triggering cytokinesis. PLoS Biol. 2012;10(9):e1001389.
12. Pereira AR, Hsin J, Krol E, Tavares AC, Flores P, Hoiczyk E, et al. FtsZ-Dependent Elongation of a Coccoid Bacterium. Mbio. 2016;7(5).

13. Kuru E, Hughes HV, Brown PJ, Hall E, Tekkam S, Cava F, et al. *In Situ* probing of newly synthesized peptidoglycan in live bacteria with fluorescent D-amino acids. Angewandte Chemie Int Ed. 2012;51(50):12519-23.
14. Jorge AM, Hoiczyk E, Gomes JP, Pinho MG. EzrA contributes to the regulation of cell size in Staphylococcus aureus. PLoS One. 2011;6(11):e27542.
15. Komis G, Mistrik M, Samajova O, Ovecka M, Bartek J, Samaj J. Superresolution live imaging of plant cells using structured illumination microscopy. Nat Protoc. 2015;10(8):1248-63.
16. Biteen JS, Thompson MA, Tselentis NK, Bowman GR, Shapiro L, Moerner WE. Super-resolution imaging in live Caulobacter crescentus cells using photoswitchable EYFP. Nat Methods. 2008;5(11):947-9.
17. Thompson RE, Larson DR, Webb WW. Precise nanometer localization analysis for individual fluorescent probes. Biophys J. 2002;82(5):2775-83.
18. Mortensen KI, Churchman LS, Spudich JA, Flyvbjerg H. Optimized localization analysis for single-molecule tracking and super-resolution microscopy. Nat Methods. 2010;7(5):377-U59.
19. Endesfelder U, Malkusch S, Fricke F, Heilemann M. A simple method to estimate the average localization precision of a single-molecule localization microscopy experiment. Histochemistry and Cell Biology. 2014;141(6):629-38.
20. Coltharp C, Kessler RP, Xiao J. Accurate Construction of Photoactivated Localization Microscopy (PALM) Images for Quantitative Measurements. PLOS ONE. 2012;7(12):e51725.
21. Palayret M, Armes H, Basu S, Watson AT, Herbert A, Lando D, et al. Virtual-'Light-Sheet' Single-Molecule Localisation Microscopy Enables Quantitative Optical Sectioning for Super-Resolution Imaging. Plos One. 2015;10(4).
22. Plank M, Wadhams GH, Leake MC. Millisecond timescale slimfield imaging and automated quantification of single fluorescent protein molecules for use in probing complex biological processes. Integr Biol. 2009;1(10):602-12.
23. Reyes-Lamothe R, Sherratt DJ, Leake MC. Stoichiometry and Architecture of Active DNA Replication Machinery in Escherichia coli. Science. 2010;328(5977):498-501.
24. Badrinarayanan A, Reyes-Lamothe R, Uphoff S, Leake MC, Sherratt DJ. In Vivo Architecture and Action of Bacterial Structural Maintenance of Chromosome Proteins. Science. 2012;338(6106):528-31.
25. Leake MC, Greene NP, Godun RM, Granjon T, Buchanan G, Chen S, et al. Variable stoichiometry of the TatA component of the twin-arginine protein transport system observed by in vivo single-molecule imaging. P Natl Acad Sci USA. 2008;105(40):15376-81.
26. Stracy M, Lesterlin C, de Leon FG, Uphoff S, Zawadzki P, Kapanidis AN. Live-cell superresolution microscopy reveals the organization of RNA polymerase in the bacterial nucleoid. P Natl Acad Sci USA. 2015;112(32):E4390-E9.
27. Wollman AJM, Leake MC. Millisecond single-molecule localization microscopy combined with convolution analysis and automated image segmentation to determine protein concentrations in complexly structured, functional cells, one cell at a time. Faraday Discuss. 2015;184:401-24.
28. Gautam S, Kim T, Spiegel DA. Chemical probes reveal an extraseptal mode of cross-linking in *Staphylococcus aureus*. Journal of the American Chemical Society. 2015;137(23):7441-7.
29. Daniel RA, Errington J. Control of Cell Morphogenesis in Bacteria: Two Distinct Ways to Make a Rod-Shaped Cell. Cell. 2003;113:767-76.
30. Haydon DJ, Stokes NR, Ure R, Galbraith G, Bennett JM, Brown DR, et al. An inhibitor of FtsZ with potent and selective anti-staphylococcal activity. Science. 2008;321(5896):1673-5.
31. Tan CM, Therien AG, Lu J, Lee SH, Caron A, Gill CJ, et al. Restoring methicillin-resistant Staphylococcus aureus susceptibility to beta-lactam antibiotics. Sci Transl Med. 2012;4(126):126ra35.
32. Giesbrecht P, Kersten T, Maidhof H, Wecke J. Staphylococcal cell wall: morphogenesis and fatal variations in the presence of penicillin. Microbiol Mol Biol Rev. 1998;62(4):1371-414.
33. Matias VR, Beveridge TJ. Cryo-electron microscopy of cell division in *Staphylococcus aureus* reveals a mid-zone between nascent cross walls. Molecular Microbiology. 2007;64(1):195-206.
34. Turner RD, Ratcliffe EC, Wheeler R, Golestanian R, Hobbs JK, Foster SJ. Peptidoglycan architecture can specify division planes in *Staphylococcus aureus*. Nature Communications. 2010;1:26.

35. Bottomley AL, Kabli AF, Hurd AF, Turner RD, Garcia-Lara J, Foster SJ. *Staphylococcus aureus* DivIB is a peptidoglycan-binding protein that is required for a morphological checkpoint in cell division. Molecular Microbiology. 2014.
36. Holden SJ, Pengo T, Meibom KL, Fernandez CF, Collier J, Manley S. High throughput 3D super-resolution microscopy reveals Caulobacter crescentus in vivo Z-ring organization. P Natl Acad Sci USA. 2014;111(12):4566-71.
37. Buss J, Coltharp C, Shtengel G, Yang XX, Hess H, Xiao J. A Multi-layered Protein Network Stabilizes the Escherichia coli FtsZ-ring and Modulates Constriction Dynamics. Plos Genet. 2015;11(4).
38. Jacq M, Adam V, Bourgeois D, Moriscot C, Di Guilmi AM, Vernet T, et al. Remodeling of the Z-Ring Nanostructure during the Streptococcus pneumoniae Cell Cycle Revealed by Photoactivated Localization Microscopy. Mbio. 2015;6(4).
39. Hussain M, Hastings JG, White PJ. A chemically defined medium for slime production by coagulase-negative staphylococci. J Med Microbiol. 1991;34(3):143-7.
40. Sambrook J, Russell DW. Molecular Cloning: A Laboratory Manual: CSHL Press; 2001.
41. Gibson DG, Young L, Chuang R-Y, Venter JC, Hutchison CA, Smith HO. Enzymatic assembly of DNA molecules up to several hundred kilobases. Nat Meth. 2009;6(5):343-5.
42. Schenk S, Laddaga RA. Improved method for electroporation of Staphylococcus aureus. FEMS Microbiology Letters. 1992;94(1-2):133-8.
43. Novick RP, Morse SI. *In vivo* Transmission of Drug Resistance Factors between Strains of *Staphylococcus aureus*. The Journal of Experimental Medicine. 1967;125(1):45-59.
44. Monahan LG, Hajduk IV, Blaber SP, Charles IG, Harry EJ. Coordinating bacterial cell division with nutrient availability: a role for glycolysis. MBio. 2014;5(3):e00935-14.
45. Lee CY, Buranen SL, Zhi-Hai Y. Construction of single-copy integration vectors for Staphylococcus aureus. Gene. 1991;103(1):101-5.
46. Horsburgh MJ, Wharton SJ, Cox AG, Ingham E, Peacock S, Foster SJ. MntR modulates expression of the PerR regulon and superoxide resistance in Staphylococcus aureus through control of manganese uptake. Molecular Microbiology. 2002;44(5):1269-86.
47. Zacharias DA, Violin JD, Newton AC, Tsien RY. Partitioning of lipid-modified monomeric GFPs into membrane microdomains of live cells. Science. 2002;296(5569):913-6.
48. Hardt P, Engels I, Rausch M, Gajdiss M, Ulm H, Sass P, et al. The cell wall precursor lipid II acts as a molecular signal for the Ser/Thr kinase PknB of Staphylococcus aureus. Int J Med Microbiol. 2017;307(1):1-10.
49. Fey PD, Endres JL, Yajjala VK, Widhelm TJ, Boissy RJ, Bose JL, et al. A genetic resource for rapid and comprehensive phenotype screening of nonessential *Staphylococcus aureus* genes. MBio. 2013;4(1):e00537-12.
50. Ong WQ, Citron YR, Schnitzbauer J, Kamiyama D, Huang B. Heavy water: a simple solution to increasing the brightness of fluorescent proteins in super-resolution imaging. Chem Commun. 2015;51(70):13451-3.
51. Huang B, Babcock H, Zhuang X. Breaking the diffraction barrier: super-resolution imaging of cells. Cell. 2010;143(7):1047-58.
52. Turner RD, Hurd AF, Cadby A, Hobbs JK, Foster SJ. Cell wall elongation mode in Gram-negative bacteria is determined by peptidoglycan architecture. Nature Communications. 2013;4:1496.
53. Huang B, Wang W, Bates M, Zhuang X. Three-Dimensional Super-Resolution Imaging by Stochastic Optical Reconstruction Microscopy. Science. 2008;319:810-3.
54. Ovesný M, Křížek P, Borkovec J, Švindrych Z, Hagen GM. ThunderSTORM: a comprehensive ImageJ plugin for PALM and STORM data analysis and super-resolution imaging. Bioinformatics. 2014;30(16):2389-90.
55. Wollman AJM, Miller H, Foster S, Leake MC. An automated image analysis framework for segmentation and division plane detection of single live Staphylococcus aureus cells which can operate at millisecond sampling time scales using bespoke Slimfield microscopy. Phys Biol. 2016;13(5).

56. Wollman AJM, Miller H, Zhou ZK, Leake MC. Probing DNA interactions with proteins using a single-molecule toolbox: inside the cell, in a test tube and in a computer. Biochem Soc T. 2015;43:139-45.
57. Leake MC, Chandler JH, Wadhams GH, Bai F, Berry RM, Armitage JP. Stoichiometry and turnover in single, functioning membrane protein complexes. Nature. 2006;443(7109):355-8.
58. Llorente-Garcia I, Lenn T, Erhardt H, Harriman OL, Liu LN, Robson A, et al. Single-molecule in vivo imaging of bacterial respiratory complexes indicates delocalized oxidative phosphorylation. Bba-Bioenergetics. 2014;1837(6):811-24.
59. Kusumi A, Sako Y, Yamamoto M. Confined Lateral Diffusion of Membrane-Receptors as Studied by Single-Particle Tracking (Nanovid Microscopy) - Effects of Calcium-Induced Differentiation in Cultured Epithelial-Cells. Biophys J. 1993;65(5):2021-40.
60. Leake MC. Analytical tools for single-molecule fluorescence imaging in cellulo. Phys Chem Chem Phys. 2014;16(25):12635-47.
61. Maki H, Miura K, Yamano Y. Katanosin B and plusbacin A_3, inhibitors of peptidoglycan synthesis in methicillin-resistant *Staphylococcus aureus*. Antimicrobial Agents and Chemotherapy. 2001;45(6):1823-7.
62. Bern M, Beniston R, Mesnage S. Towards an automated analysis of bacterial peptidoglycan structure. Analytical and Bioanalytical Chemistry. 2016.
63. Komatsuzawa H, Sugai M, Nakashima S, Yamada S, Matsumoto A, Oshida T, et al. Subcellular localization of the major autolysin, ATL and its processed proteins in Staphylococcus aureus. Microbiol Immunol. 1997;41(6):469-79.
64. Touhami A, Jericho MH, Beveridge TJ. Atomic force microscopy of cell growth and division in *Staphylococcus aureus*. Journal of Bacteriology. 2004;186(11):3286-95.
65. Horsburgh MJ, Aish JL, White IJ, Shaw L, Lithgow JK, Foster SJ. sigmaB modulates virulence determinant expression and stress resistance: characterization of a functional rsbU strain derived from Staphylococcus aureus 8325-4. J Bacteriol. 2002;184(19):5457-67.
66. Kreiswirth BN, Lofdahl S, Betley MJ, O'Reilly M, Schlievert PM, Bergdoll MS, et al. The toxic shock syndrome exotoxin structural gene is not detectably transmitted by a prophage. Nature. 1983;305(5936):709-12.
67. Kuroda M, Ohta T, Uchiyama I, Baba T, Yuzawa H, Kobayashi I, et al. Whole genome sequencing of meticillin-resistant Staphylococcus aureus. Lancet. 2001;357(9264):1225-40.
68. Aish JL. Environmental regulation of virulence determinant expression in *Staphylococcus aureus*: University of Sheffield; 2003.

Appendix I

Appendix I -Table 1. Strains used in this study.

Strain	**Relevant Genotype/markers**	**Source**
SH1000	Functional *rsbU*- derivative of 8325-4	(65)
RN4220	Restriction deficient transformation recipient	(66)
CYL316	*S. aureus* RN4220 pCL112Δ19 (cm)	(45)
JGL227	*S. aureus* SH1000 *ezrA-gfp+* (ery)	(10)
SH4386	*S. aureus* SH1000 *ezrA-eyfp* (kan)	This study
SH4388	*S. aureus* SH1000 *ezrA-eyfp ΔezrA* (kan, tet)	This study
SH4603	*S. aureus* SH1000 *ezrA-meyfp* (kan)	This study
SH4604	*S. aureus* SH1000 *ezrA-meyfp ΔezrA* (kan, tet)	This study

SH4639	*S. aureus* SH1000 *ezrA-gfp* (kan)	This study
SH4640	*S. aureus* SH1000 *ezrA-gfp ΔezrA* (kan, tet)	This study
SH4641	*S. aureus* SH1000 *ezrA-snap* (kan)	This study
SH4642	*S. aureus* SH1000 *ezrA-snap ΔezrA* (kan, tet)	This study
SH4652	*S. aureus* SH1000 *ezrA-eyfp ΔezrA* pCQ11-FtsZ-SNAP (kan, tet, ery)	This study
SH4665	*S. aureus* SH1000 pCQ11-FtsZ-eYFP (ery)	This study
NE679	*S. aureus* JE2 with transposon insertion in *pbp4* (ery)	(49)
SH4425	*S. aureus* SH1000 *pbp4* (ery)	This study
N315	Methicillin-resistant *S. aureus*	(67)
SU492	*B. subtilis* SU5 P_{xyl}-*ftsZ-yfp* (spec)	(44)

867 Appendix I -Table 2. Plasmids used in this study

Plasmid	Relevant Genotype/markers	Source
pGM074	pKASBAR-kan(35) carrying *ezra-psmorange* under the putative *ezrA* promoter (amp, kan)	G. McVicker
pSNAP-tag (T7)-2	*E. coli* expression plasmid carrying the *snap* gene under the control of the T7 promoter (amp)	New England Biolabs
pOB	pGEM3Zf(+) cloning vector containing the erythromycin resistance cassette (amp, ery)	(46)
pAISH	TetR derivative of pMUTIN4	(68)
pKASBAR-EzrA-eYFP	pKASBAR-kan containing *ezrA-eyfp* under the putative *ezrA* promoter (amp, kan)	This study
pKASBAR-EzrA-meYFP	pKASBAR-kan containing *ezrA-meyfp* under the putative *ezrA* promoter (amp, kan)	This study
pKASBAR-EzrA-GFP	pKASBAR-kan containing *ezrA-gfp* under the putative *ezrA* promoter (amp, kan)	This study
pKASBAR-EzrA-SNAP	pKASBAR-kan containing *ezrA-snap* under the putative *ezrA* promoter (amp, kan)	This study
pOB-*ΔezrA*	pOB containing the *ezrA* deletion cassette consisting of a 1.5 kb fragment of the upstream region of *S. aureus ezrA*, the tetracycline resistance cassette from pAISH and a1.5 kb fragment of the downstream region of *S. aureus ezrA* (amp, ery, tet)	This study
pSS26b	pUC19 encoding *snap* (amp)	Covalys
pSS26bFtsZ-C	pSS26b containing *ftsZ-snap* (amp)	This study

pCQ11	*E. coli-S. aureus* shuttle vector containing *lacI*, Pspac and *gfp* (amp, ery)	(48)
pCQ11-FtsZ-SNAP	pCQ11 derivative containing *ftsZ-snap* under Pspac (amp, ery)	This study
pCQ11-FtsZ-eYFP	pCQ11-FtsZ-SNAP with *eyfp* replacement of *snap* (amp, ery)	This study

868 Appendix I -Table S3. Oligonucleotides used in this study.

Oligonucleotide name	Sequence (5' to 3')
eYFP-F	CGGCGCGCCTCAGGTTCAGGTTCAGGTATGGTGAGCAAGGGCGAG
eYFP-R	CGCGGCCGCTTACTTGTACAGCTCGTCCATGCCGAGAGTGATCCCGGC
GFP-F	CGGCGCGCCTCAGGTTCAGGTTCAGGTATGGCTAGCAAAGGAGAAGAA CTTTTCACTGGAGTTGTCCC
GFP-R	CGCGGCCGCTTATTTGTAGAGCTCATCCATGCCATGTGTAATCCCAGCA GC
SNAP-F	GGGCGCGCCTCAGGTTCAGGTTCAGGTATGGACAAAGACTGCGAAATGA AGCGCAC
SNAP-R	CGAATTCTCATTAACCCAGCCCAGGCTTGCCCAGTCTG
meYFP-F	CTACCAGTCCAAGCTGAGCAAAGAC
meYFP-R	CTCAGGTAGTGGTTGTCG
pOB-ezrA-up-F	TTTACGTACACTATCTGCAGATGCTTCTCCTCCTAATTTATCATT
pOB-ezrA-up-R	ATTCGAGCTCGGTACCCGGGTTTTAAATTAATAAAAAAAACACCCACAATT
pOB-ezrA-down-F	CACTATAGAATACTCAAGCTTACTCCTTAATTTCCTCATAAATGATGA
pOB-ezrA-down-R	GGATCAACTTTGGGAGAGAGAAACTAGTATGTAGTTATACTTAAATAATAT GAGC
pOB-TetR-F	TAAATTAGGAGGAGAAGCATCTGCAGATAGTGTACGTAAAAAGA
pOB-TetR-R	GTATAACTACATACTAGTTTCTCTCTCCCAAAGTTGATCCC
ftsZ-eyfp-F	ACATGGCCATGTCAGGTTCAG
ftsZ-eyfp-R	GGCGCGCCTTATTTATATAATTC
FGFtsZXhoI-F	CTCGAGATGTTAGAATTTGAACAAGG
FGFtsZEcoRI-R	TTAGAATTCACGTCTTGTTCTTCTTGAA
FGFtsZNheI-F	GTTGCTAGCATGTTAGAATTTGAACAAGG
FGFtsZAscI-R	GTTGGCGCGCCTTATCCCAGACCCGGTTTAC

869
870

a

EzrA-eYFP SH4388 (*ezrA-eyfp ΔezrA*)

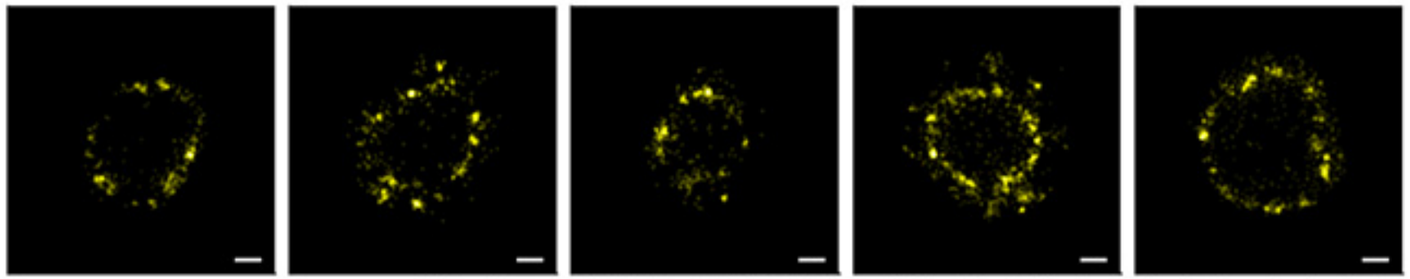

b

FtsZ-eYFP SH4665 (pCQ11-FtsZ-eYFP)

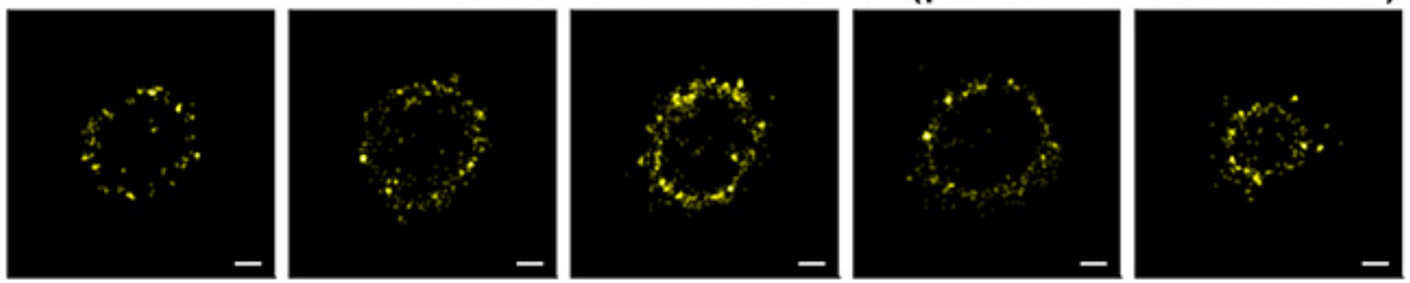

c

Simulations

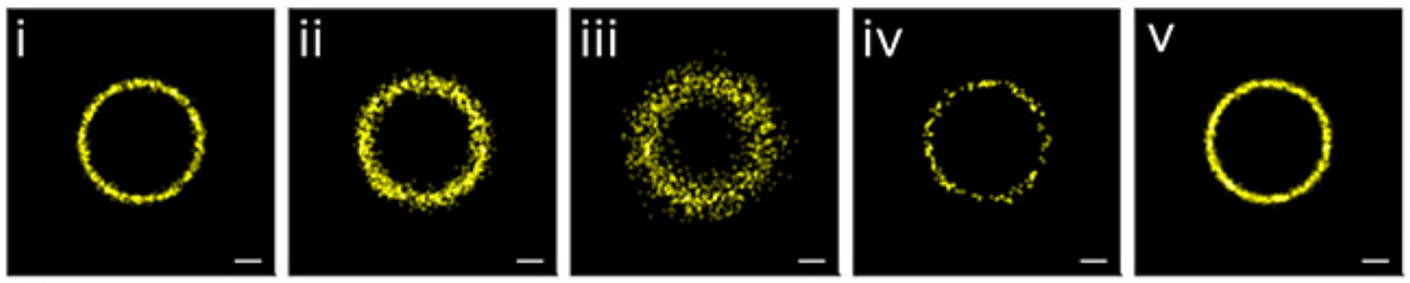

d

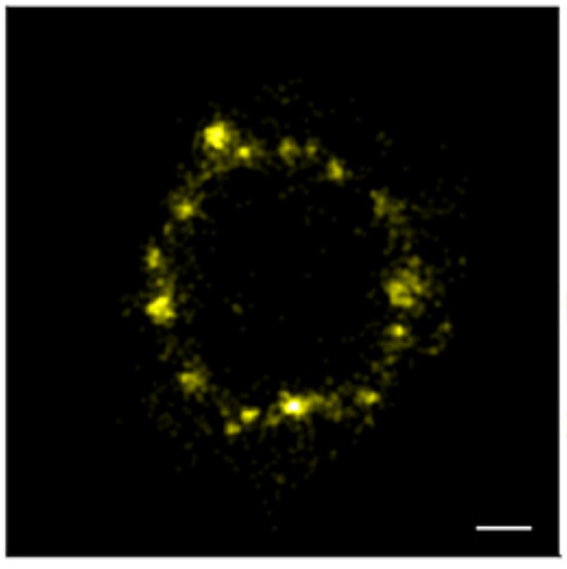

e

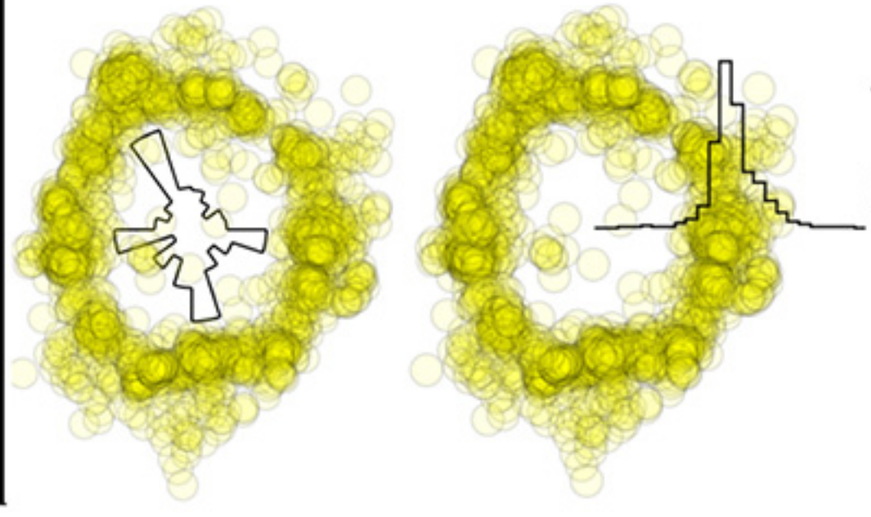

f

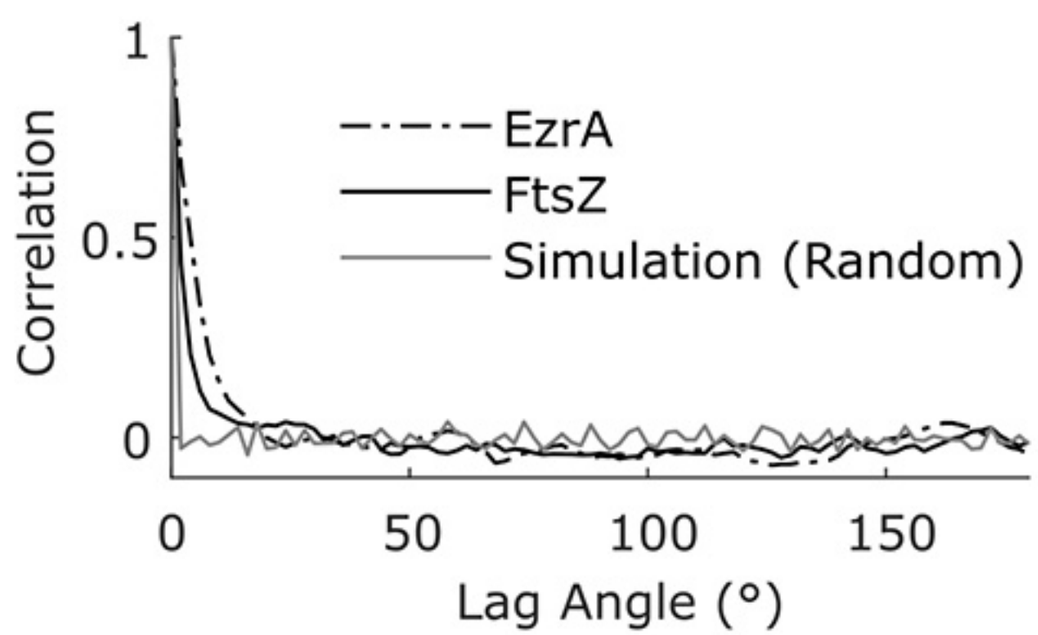

g

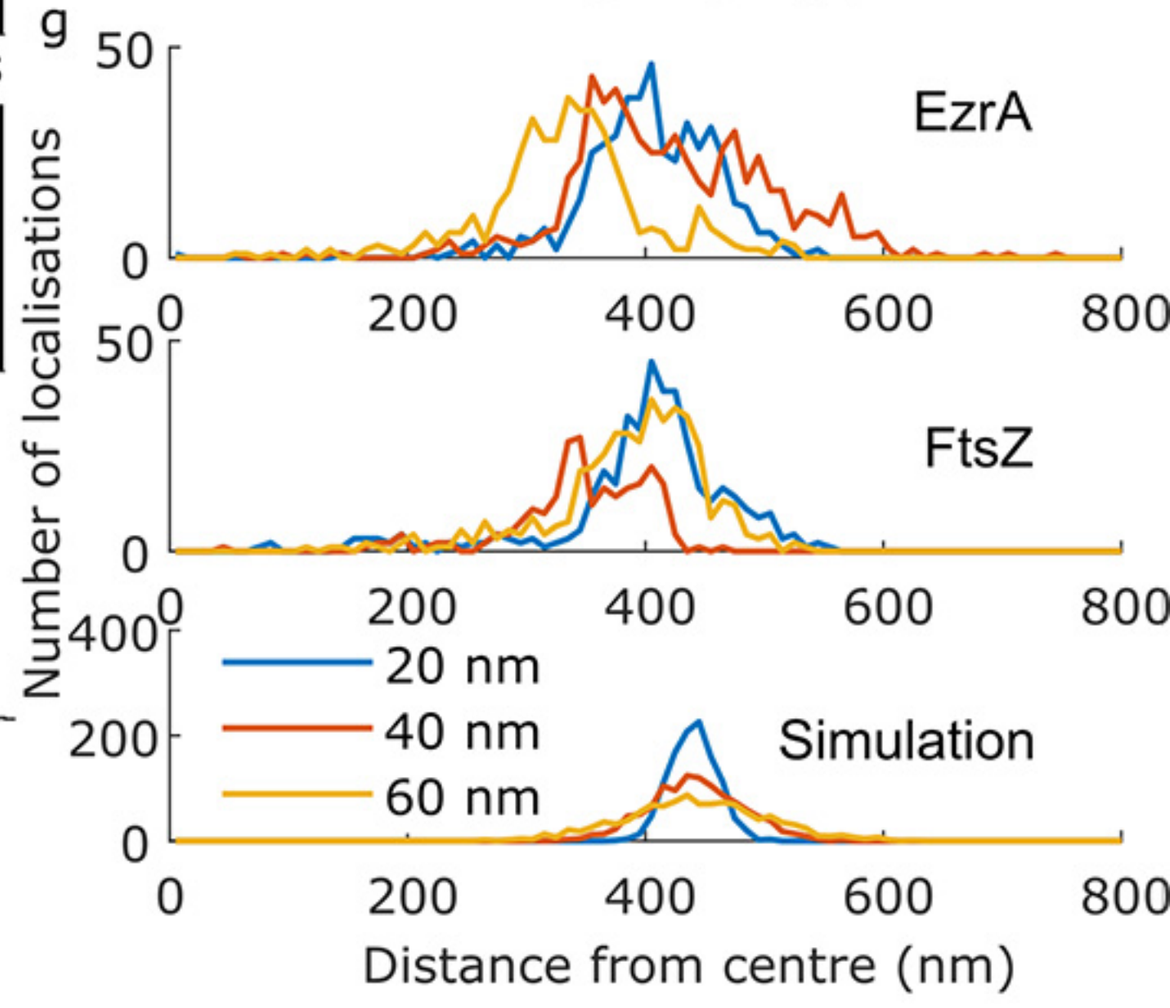

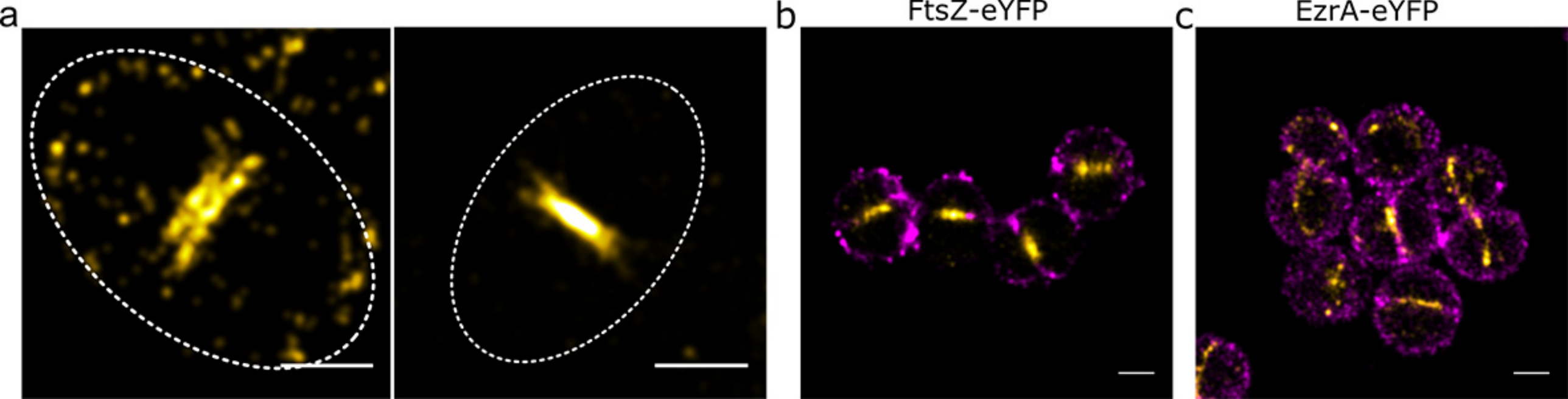
a
b
FtsZ-eYFP
c
EzrA-eYFP

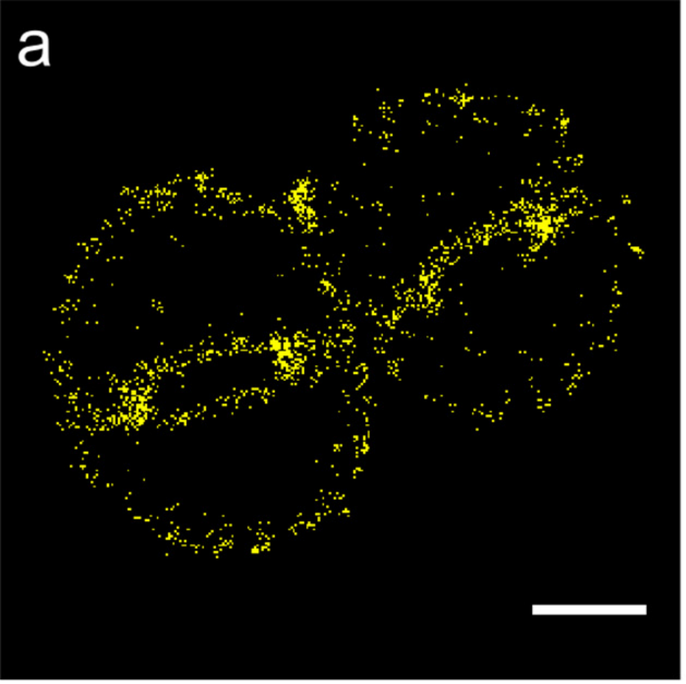
a

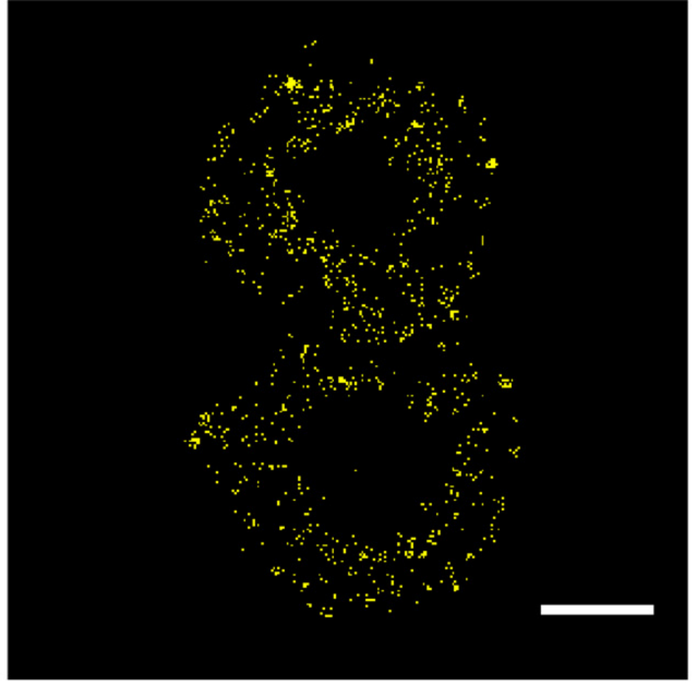

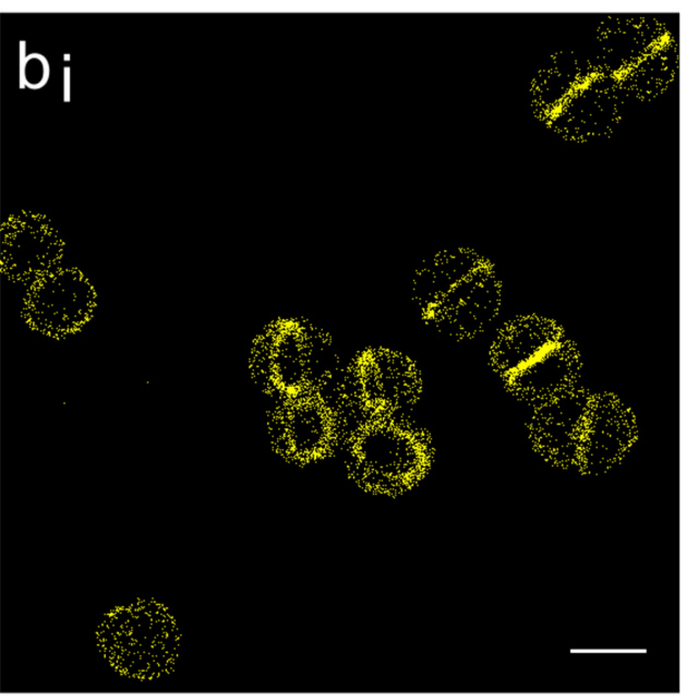
bi

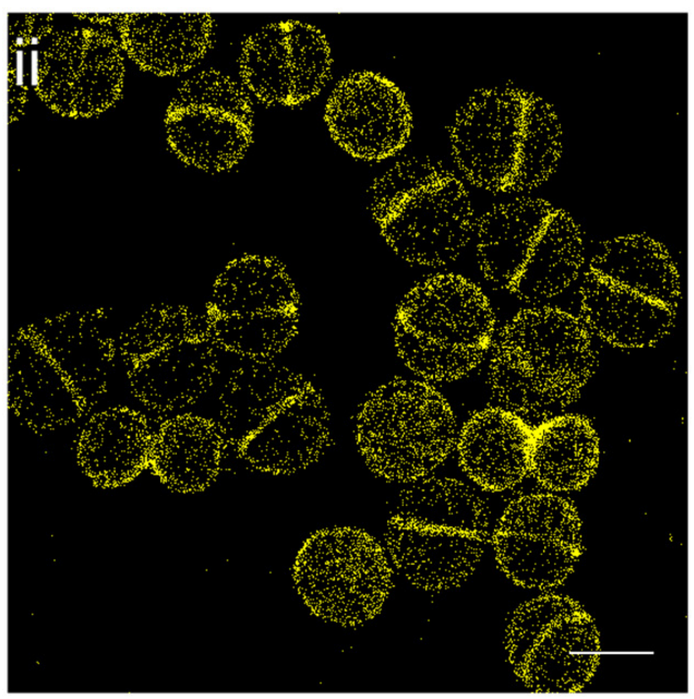
ii

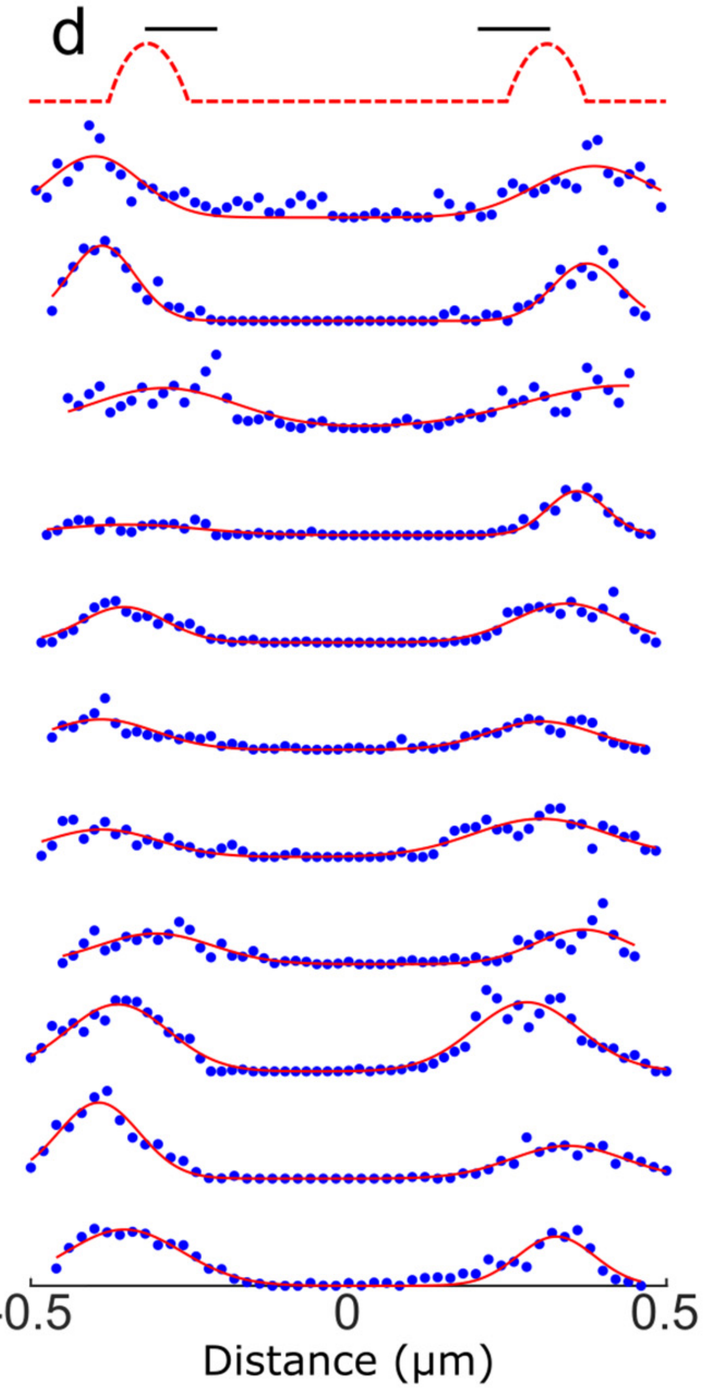
d
-0.5
0
0.5
Distance (μm)

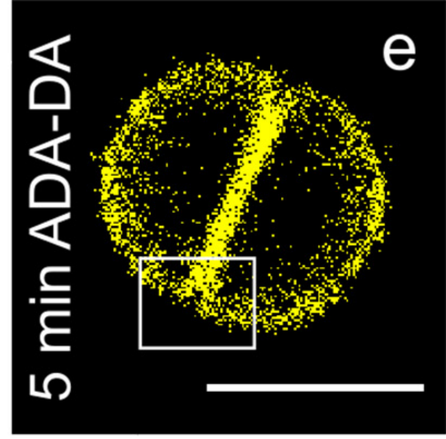
5 min ADA-DA
e

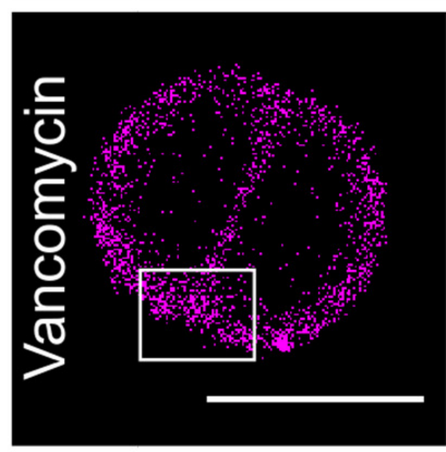
Vancomycin

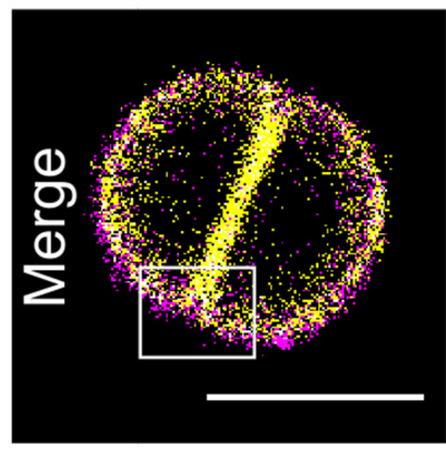
Merge

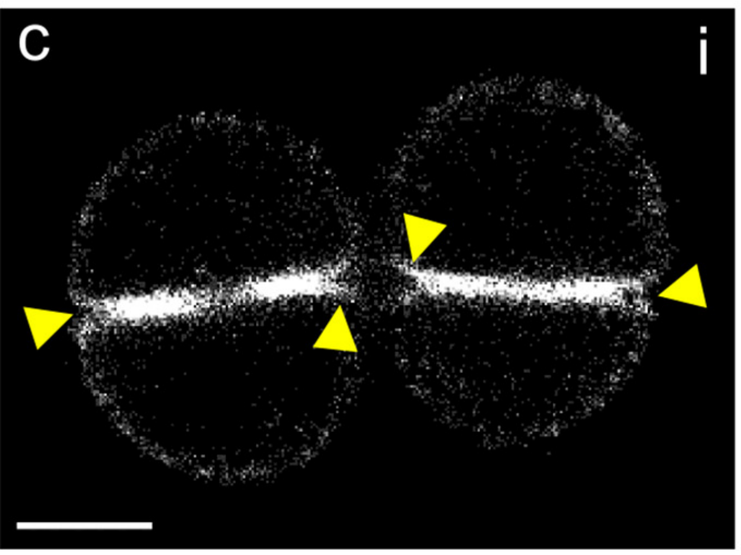
c
i

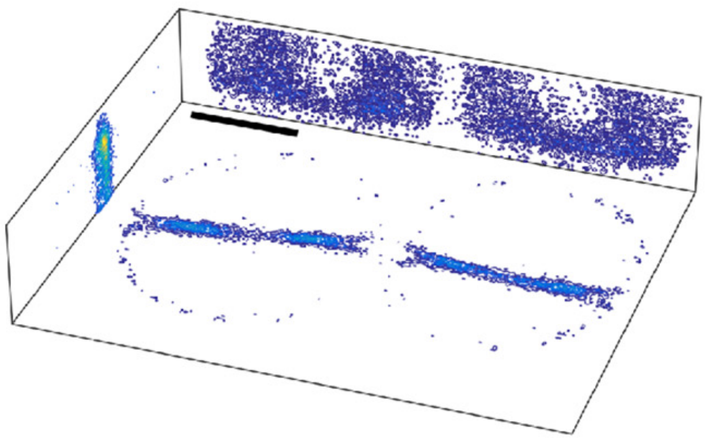

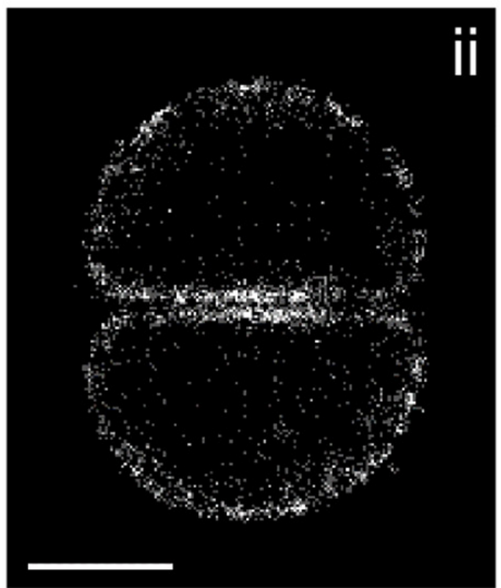
ii

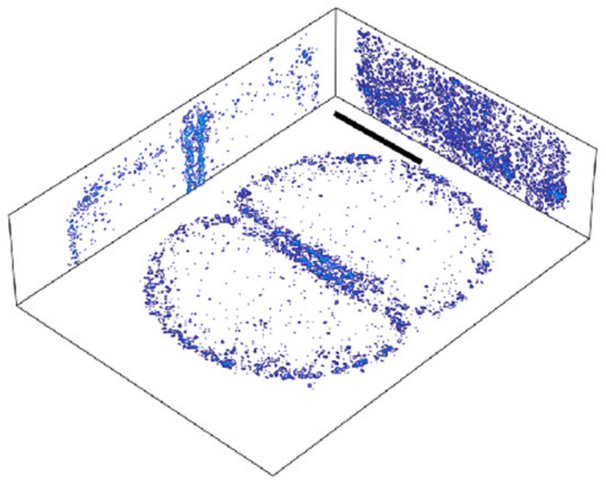

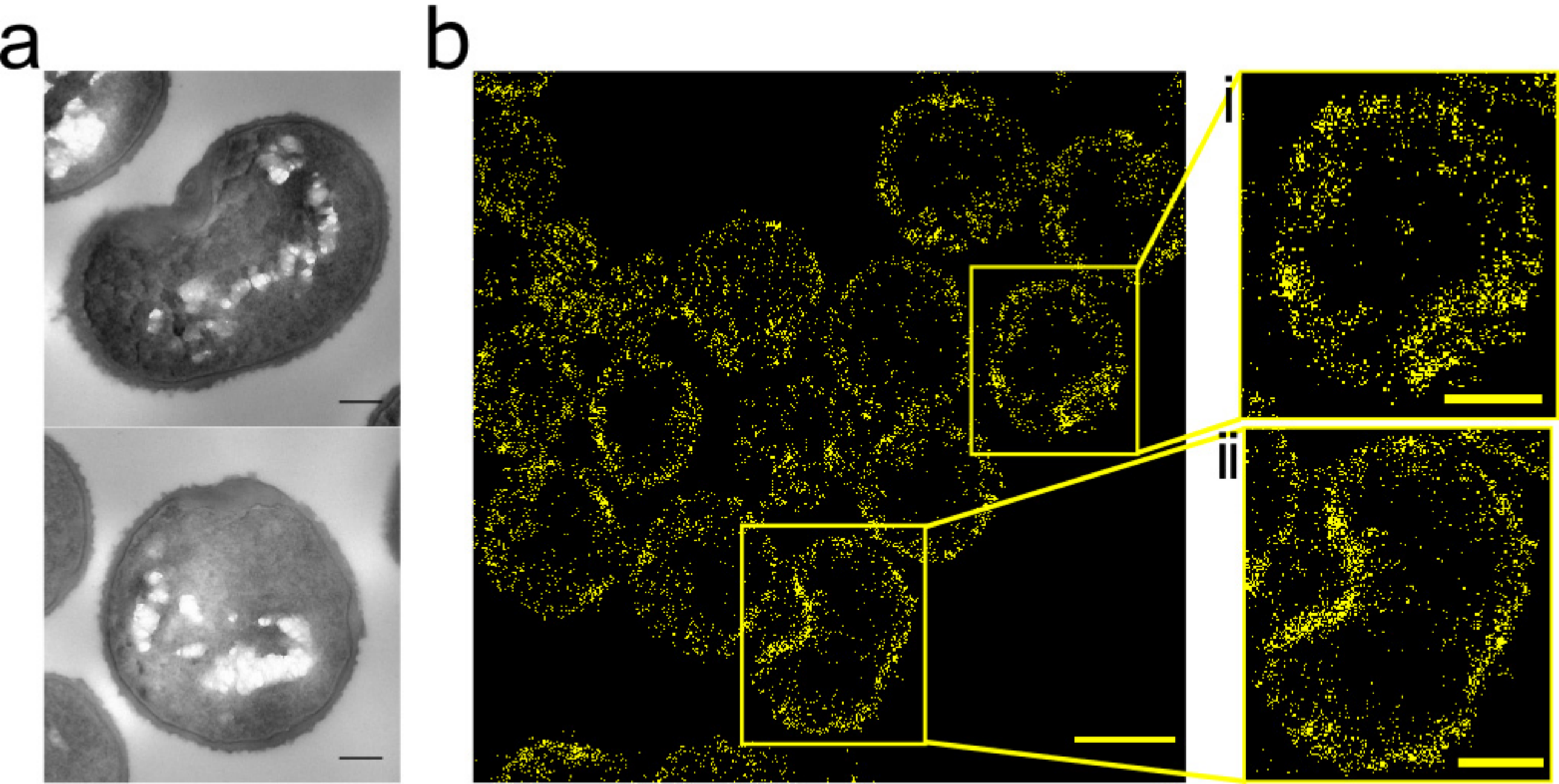
a
b
i
ii

a

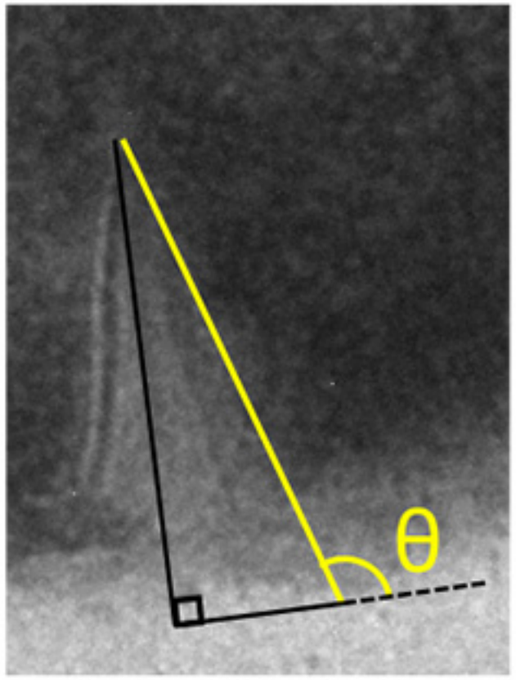
θ

b

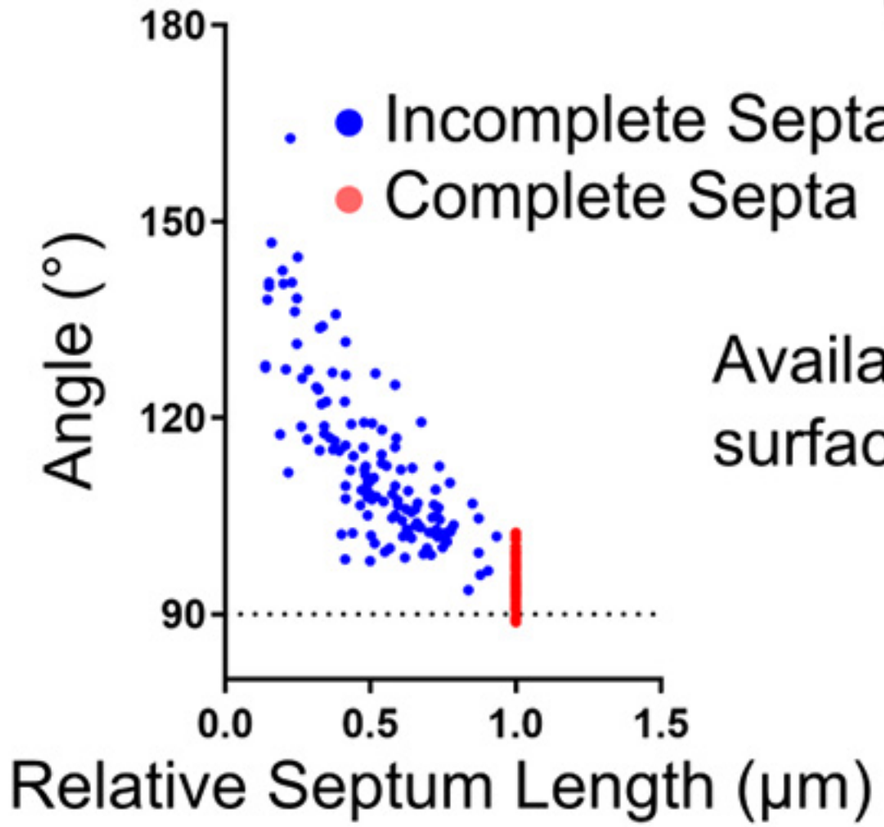
180
150
120
90
Angle (°)
Incomplete Septa
Complete Septa
0.0
0.5
1.0
1.5
Relative Septum Length (μm)

c

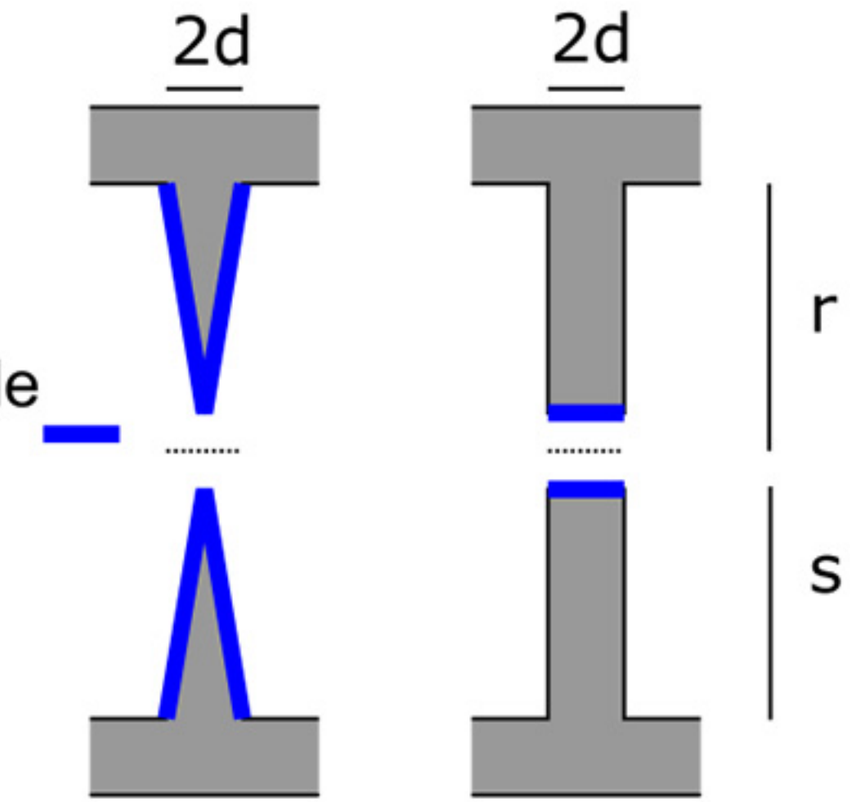
2d
2d
Available surface
r
s

d

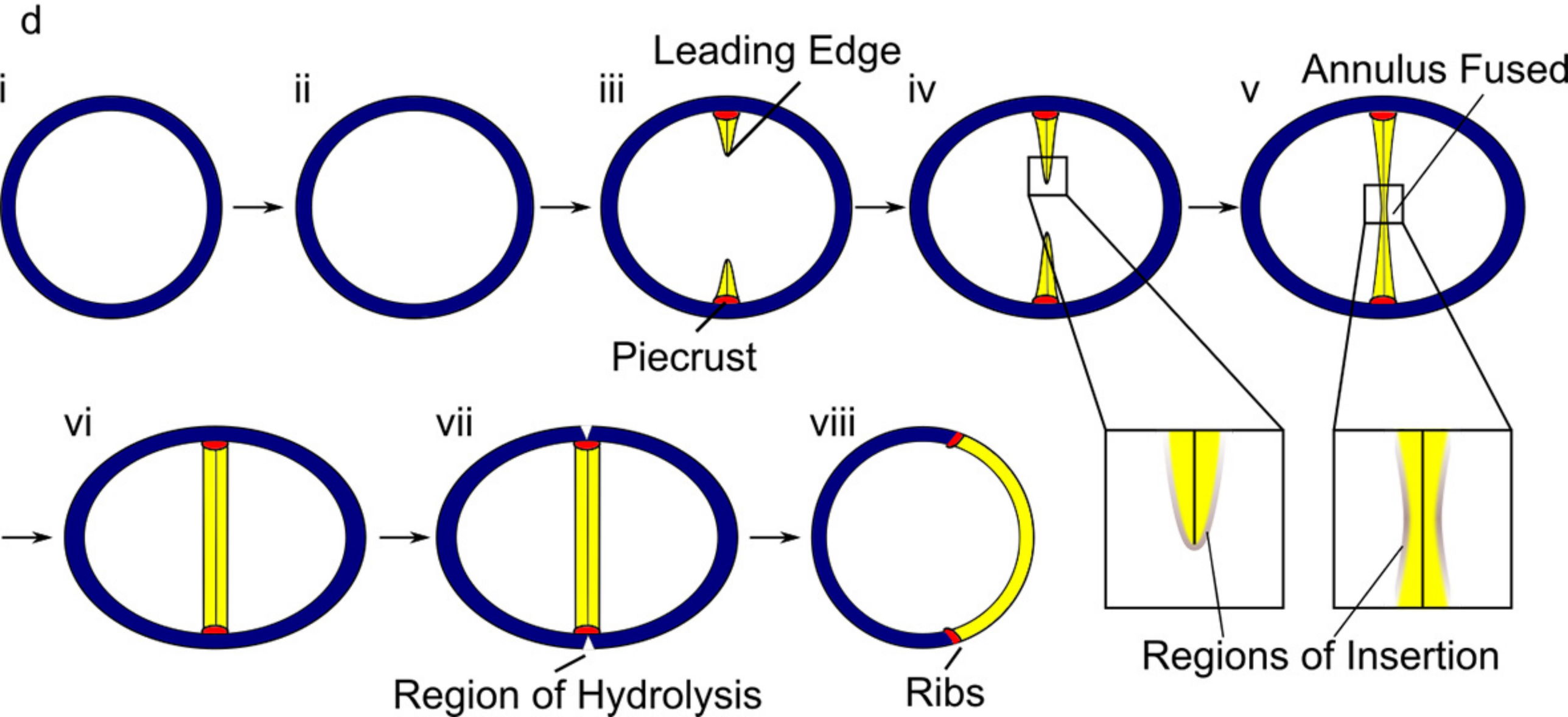
i
ii
iii
Leading Edge
iv
v
Annulus Fused
Piecrust
vi
vii
viii
Region of Hydrolysis
Ribs
Regions of Insertion

a

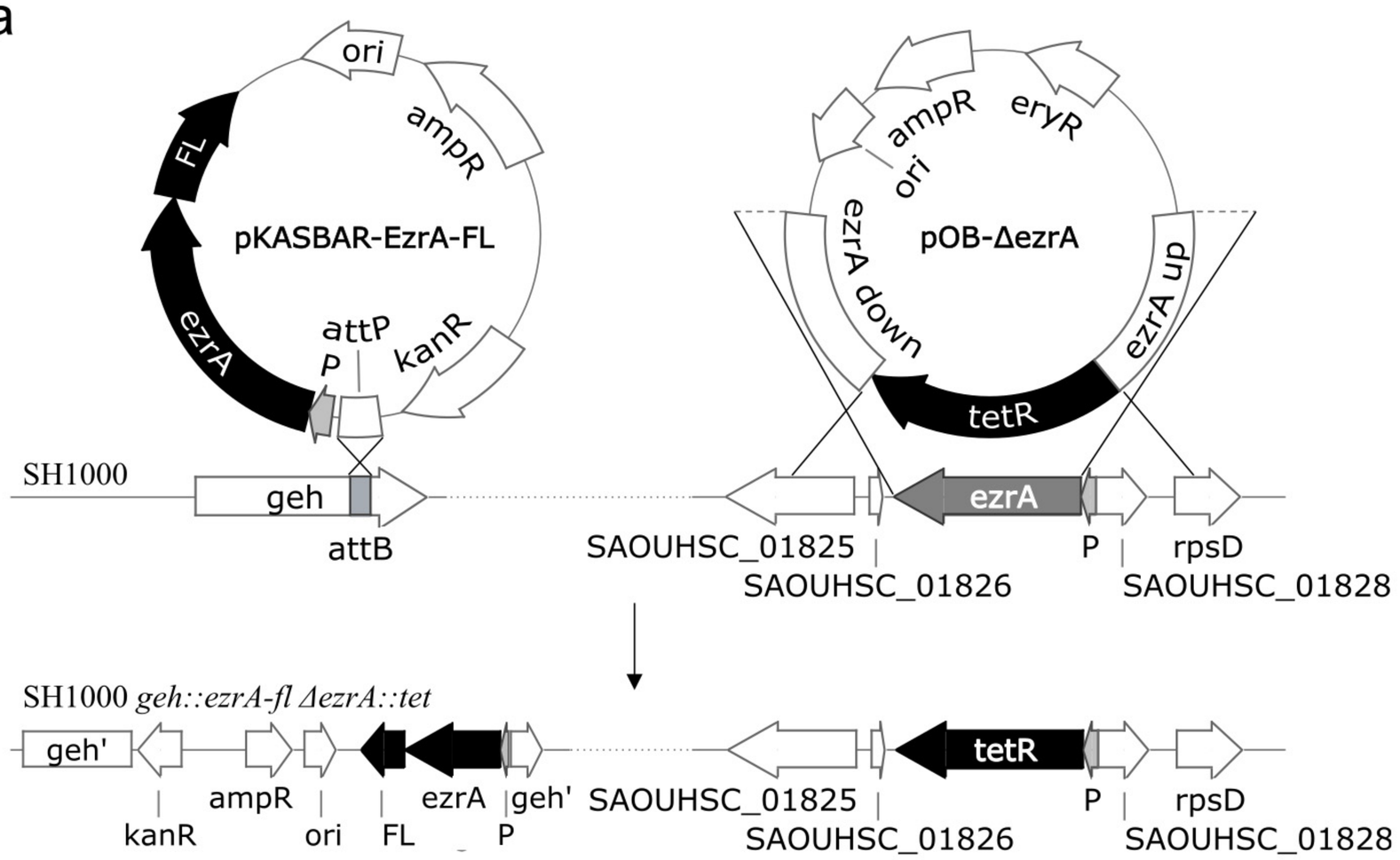
ori
ampR
FL
pKASBAR-EzrA-FL
ezrA
attP
P
kanR
SH1000
geh
attB
ampR
eryR
ori
pOB-ΔezrA
ezrA down
ezrA up
tetR
ezrA
SAOUHSC_01825
SAOUHSC_01826
P
rpsD
SAOUHSC_01828
SH1000 geh::ezrA-fl ΔezrA::tet
geh'
tetR
ampR
ori
kanR
ezrA
FL
geh'
P
SAOUHSC_01825
SAOUHSC_01826
P
rpsD
SAOUHSC_01828

b

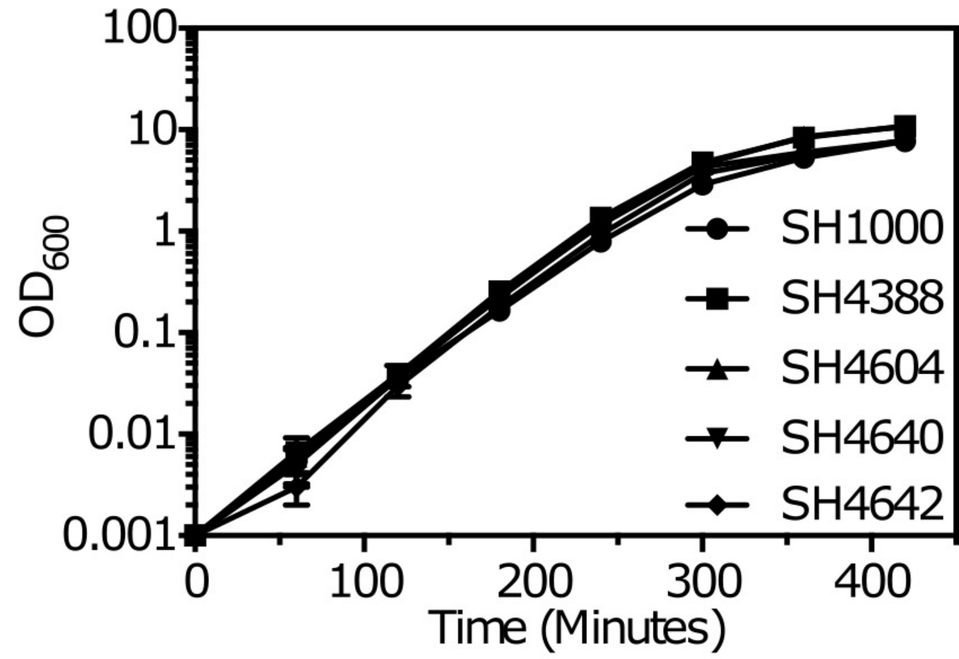
100
10
1
0.1
0.01
0.001
OD600
0
100
200
300
400
Time (Minutes)
SH1000
SH4388
SH4604
SH4640
SH4642

c

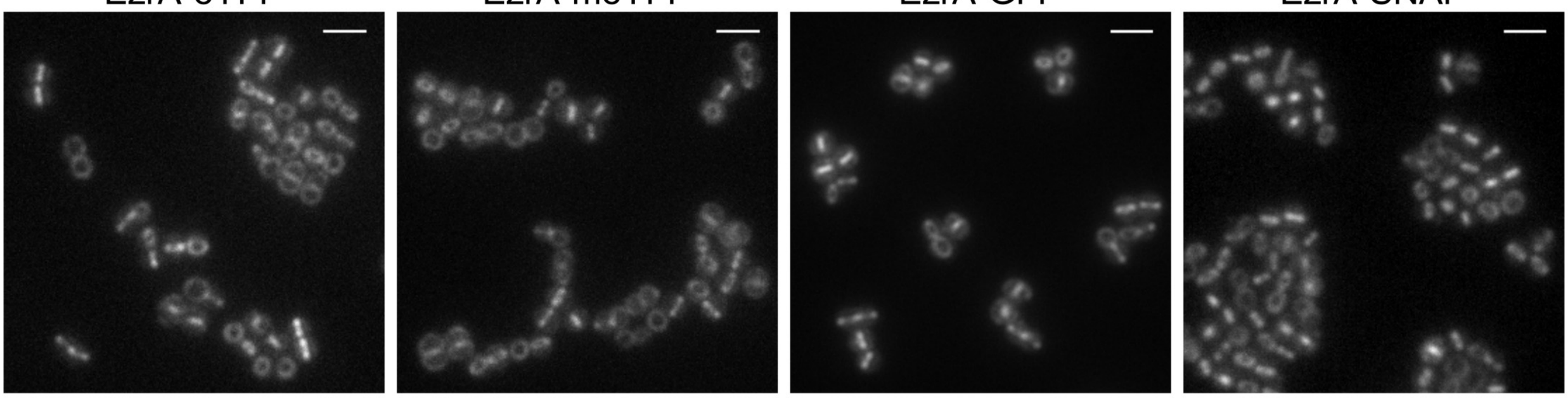
EzrA-eYFP
EzrA-meYFP
EzrA-GFP
EzrA-SNAP

d

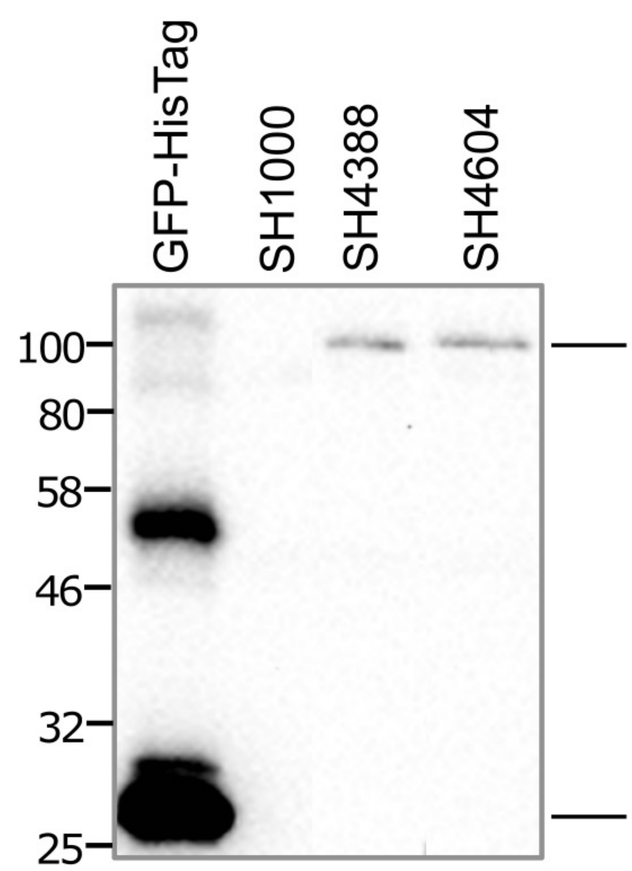
GFP-HisTag
SH1000
SH4388
SH4604
100
80
58
46
32
25

e

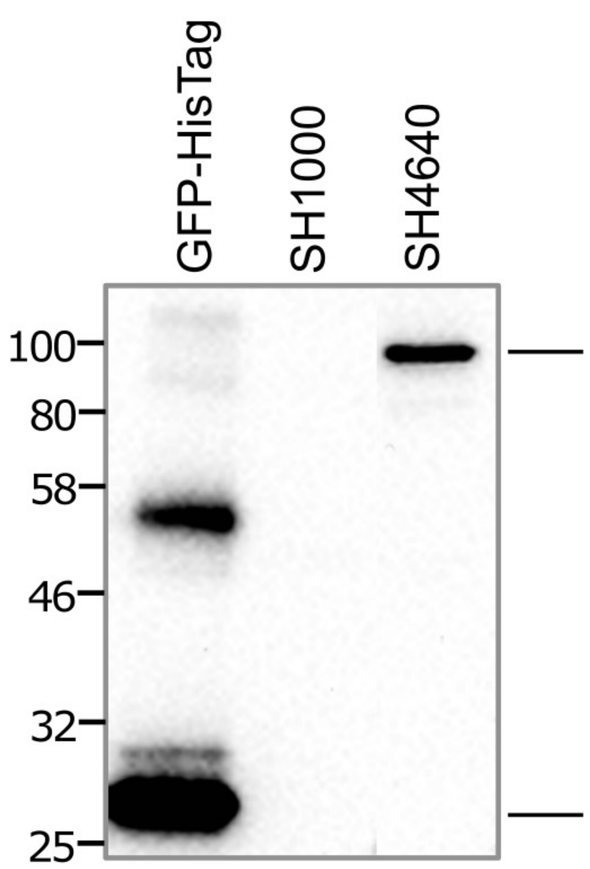
GFP-HisTag
SH1000
SH4640
100
80
58
46
32
25

f

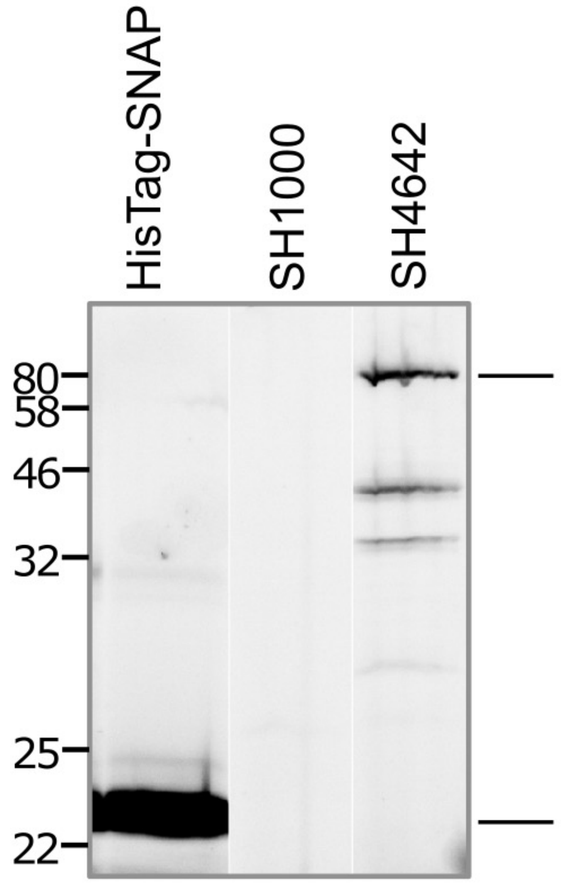
HisTag-SNAP
SH1000
SH4642
80
58
46
32
25
22

a

i

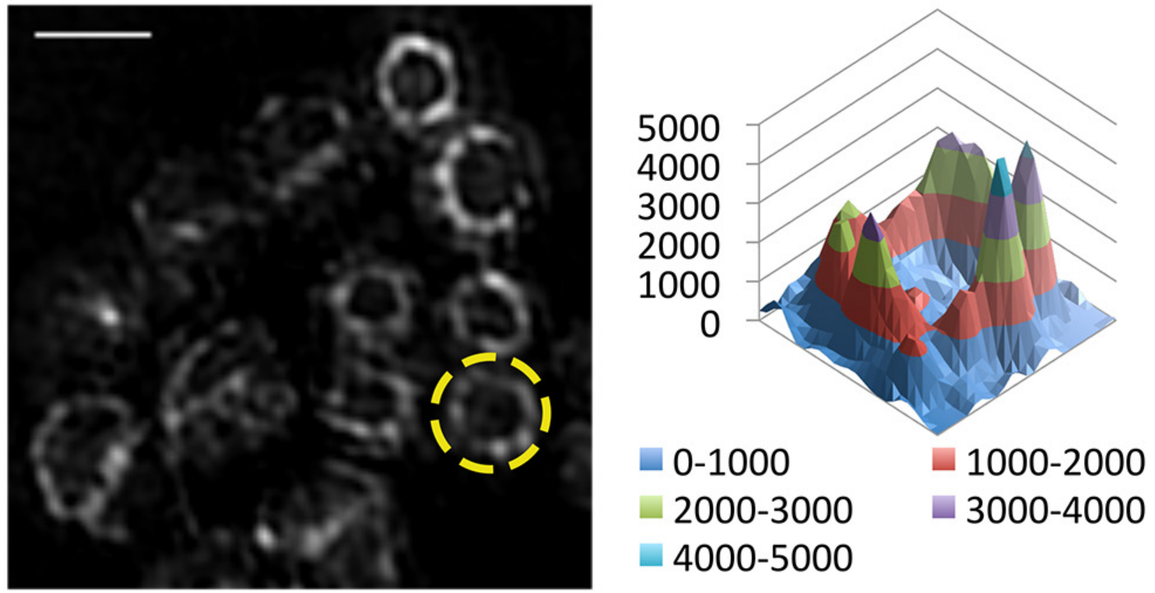
5000
4000
3000
2000
1000
0
0-1000
1000-2000
2000-3000
3000-4000
4000-5000

ii

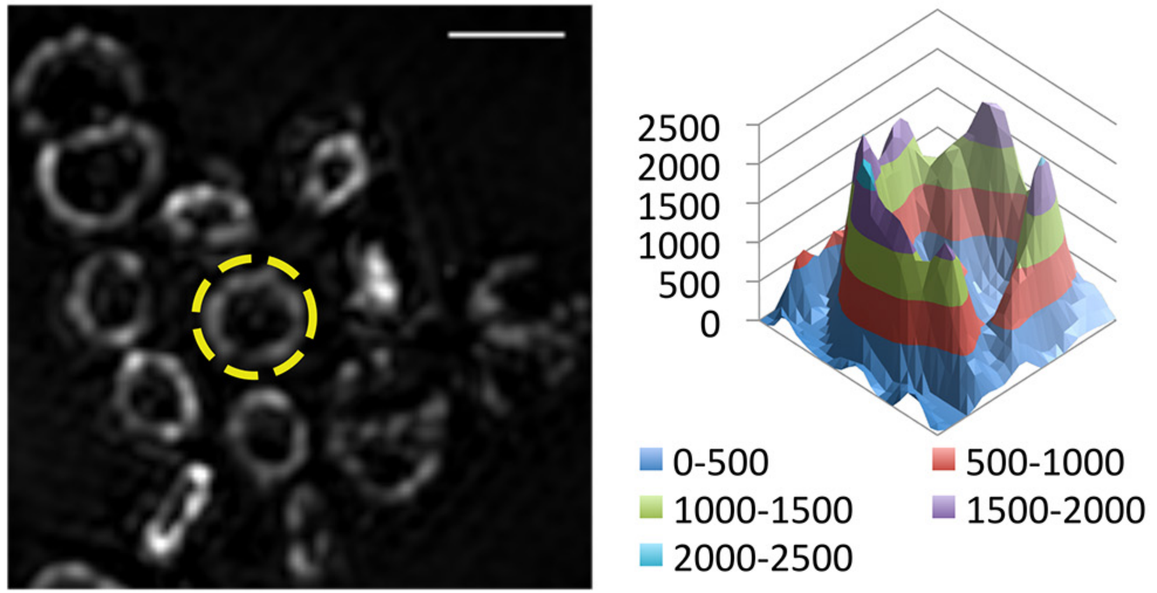
2500
2000
1500
1000
500
0
0-500
500-1000
1000-1500
1500-2000
2000-2500

b

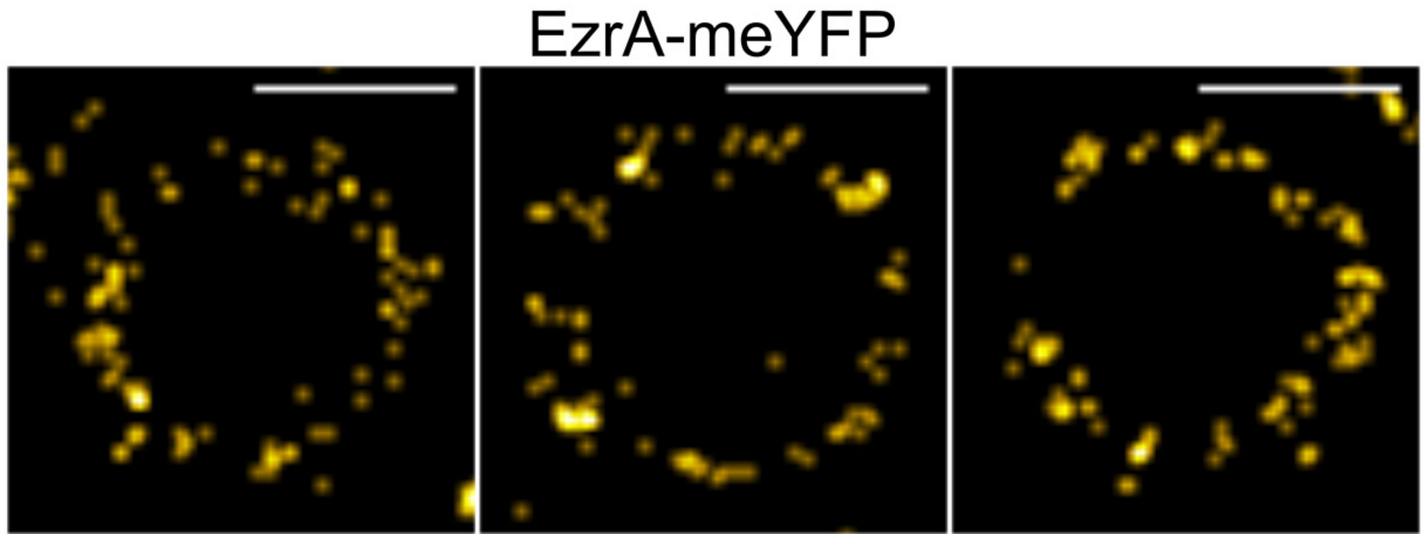
EzrA-meYFP

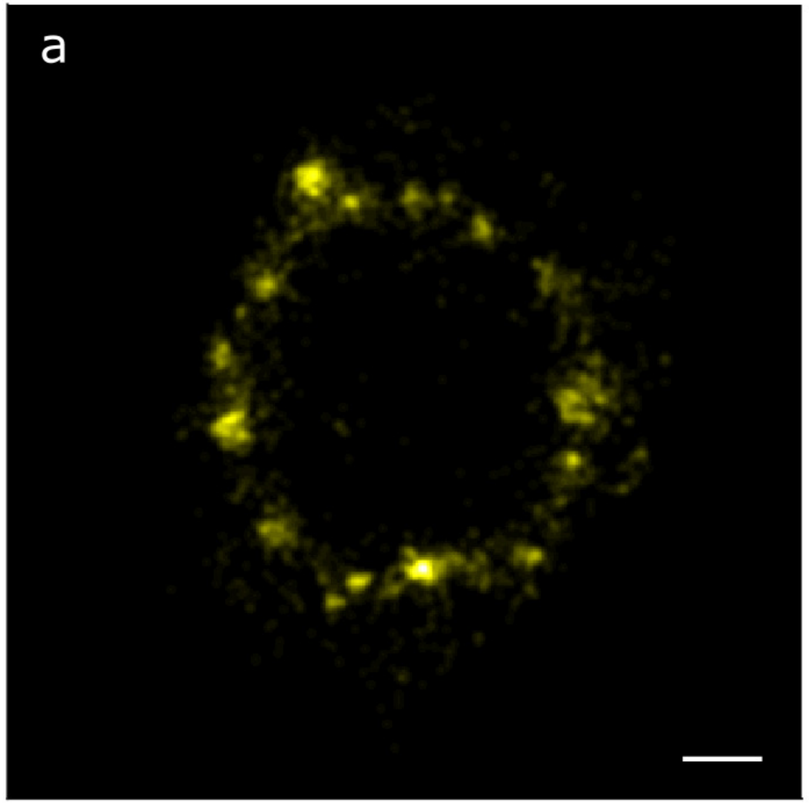
a

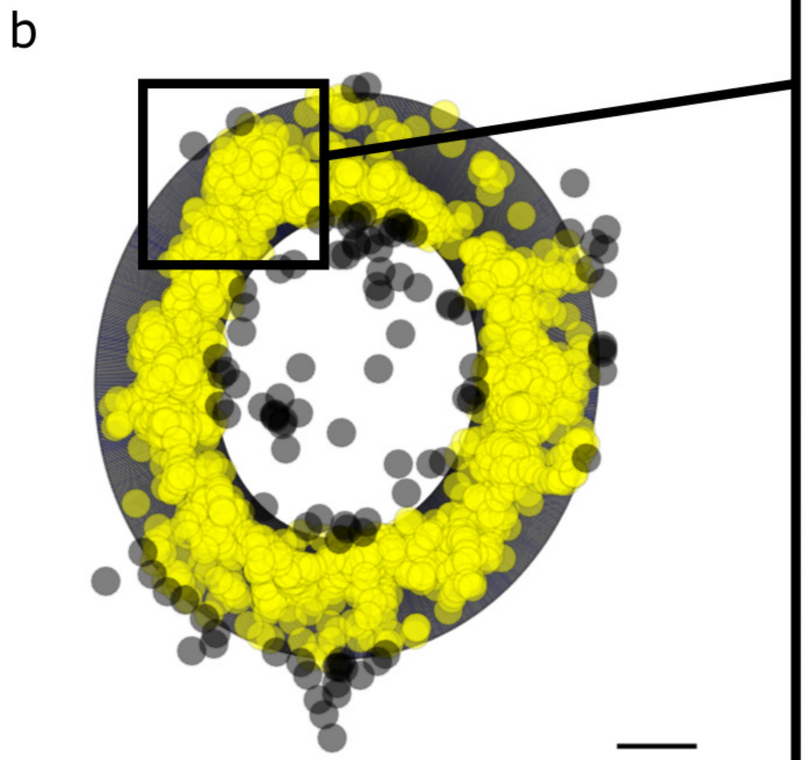
b

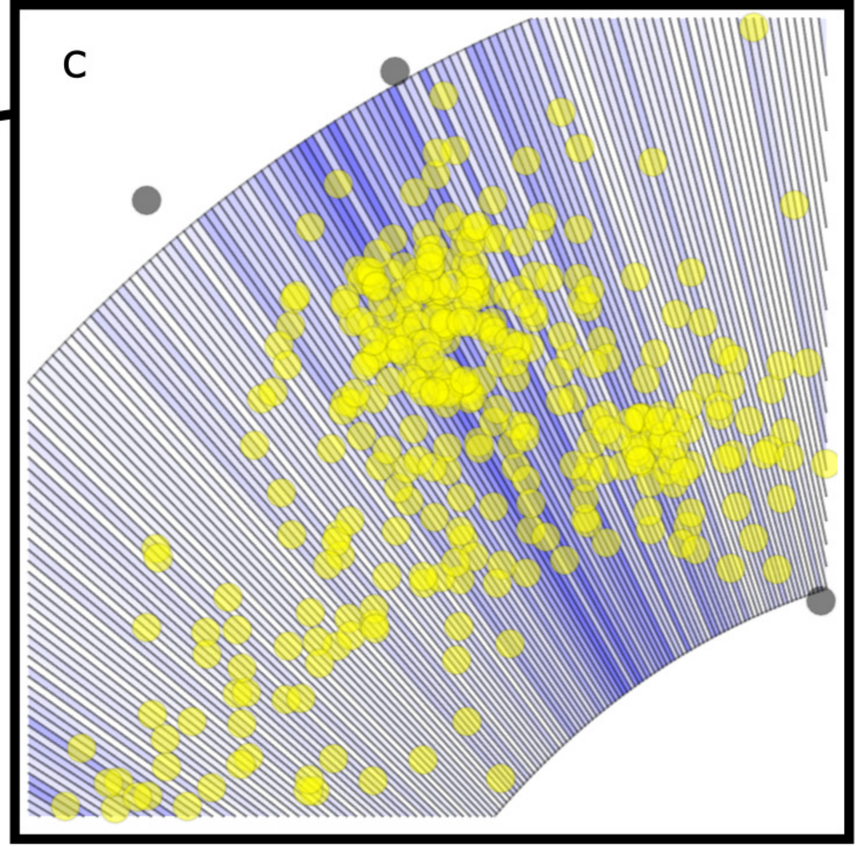
c

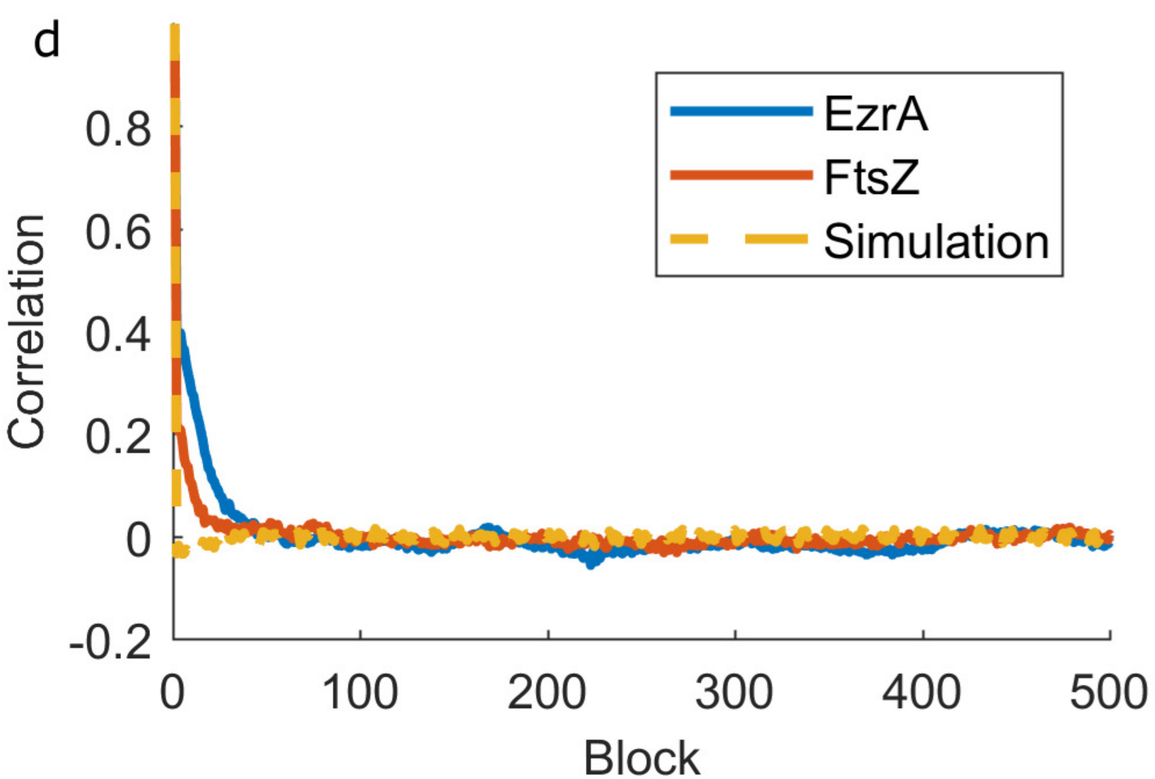
d
Correlation
0.8
0.6
0.4
0.2
0
-0.2
0
100
200
300
400
500
Block
EzrA
FtsZ
Simulation

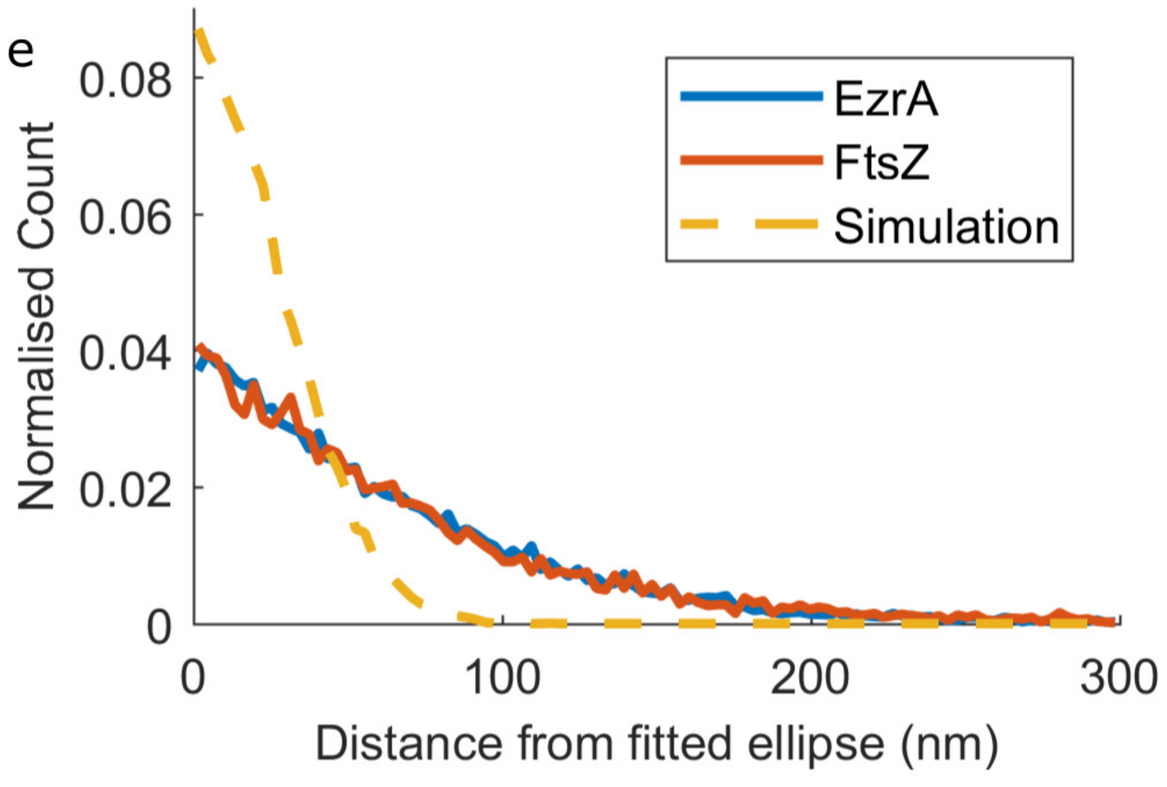
e
Normalised Count
0.08
0.06
0.04
0.02
0
0
100
200
300
Distance from fitted ellipse (nm)
EzrA
FtsZ
Simulation

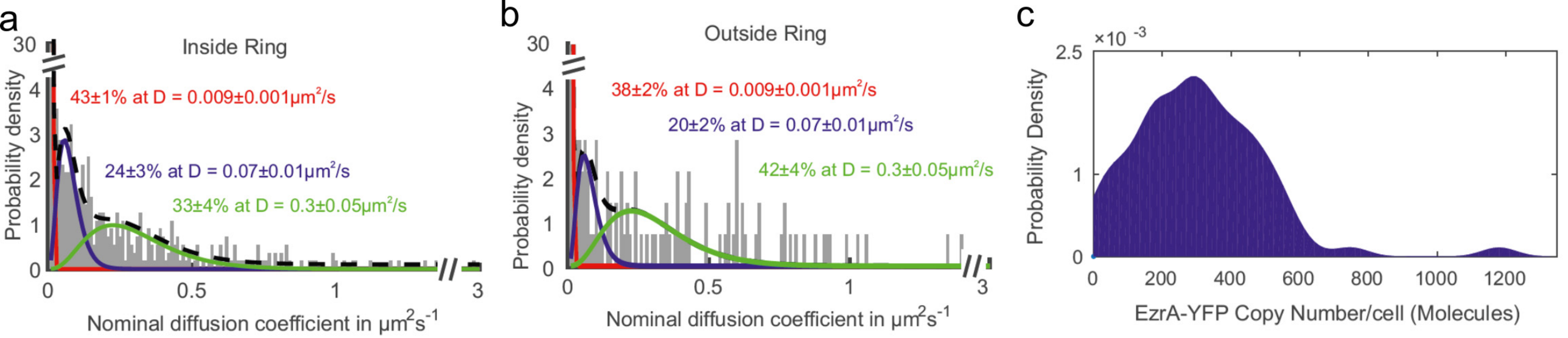
a
Inside Ring
43±1% at D = 0.009±0.001μm²/s
24±3% at D = 0.07±0.01μm²/s
33±4% at D = 0.3±0.05μm²/s
Probability density
Nominal diffusion coefficient in μm²s⁻¹
b
Outside Ring
38±2% at D = 0.009±0.001μm²/s
20±2% at D = 0.07±0.01μm²/s
42±4% at D = 0.3±0.05μm²/s
Probability density
Nominal diffusion coefficient in μm²s⁻¹
c
×10⁻³
Probability Density
EzrA-YFP Copy Number/cell (Molecules)

a

Total Ion Count

i

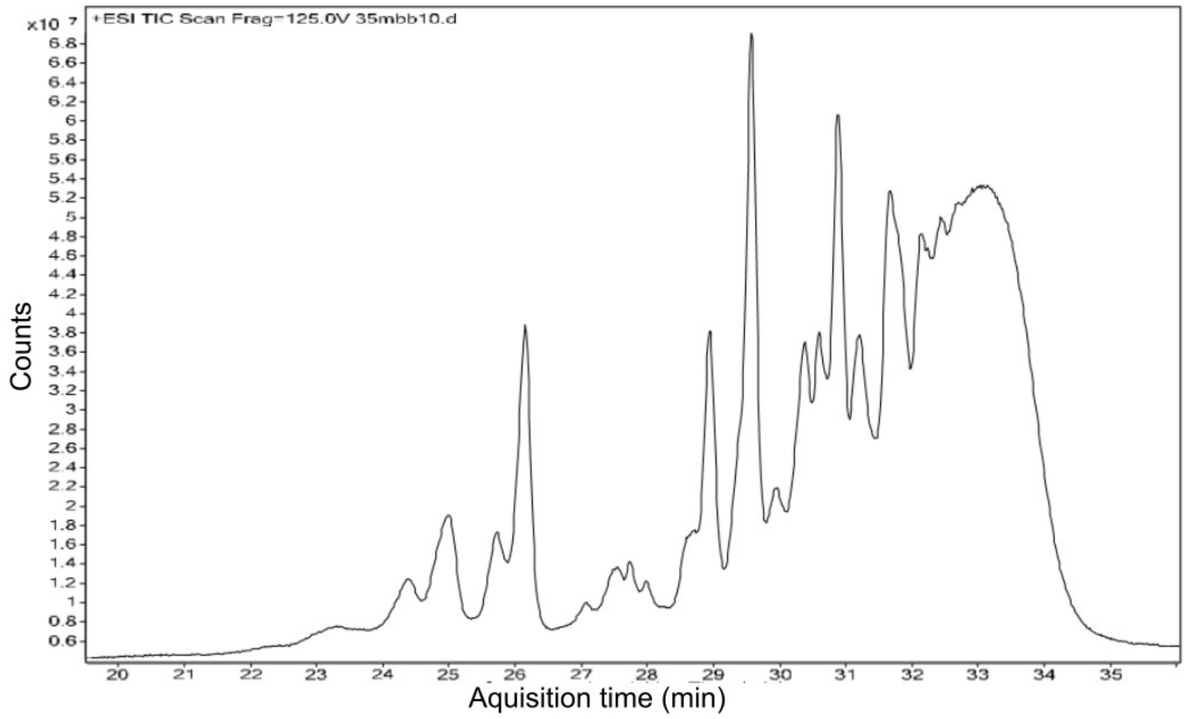

Extracted Ion Count

ii

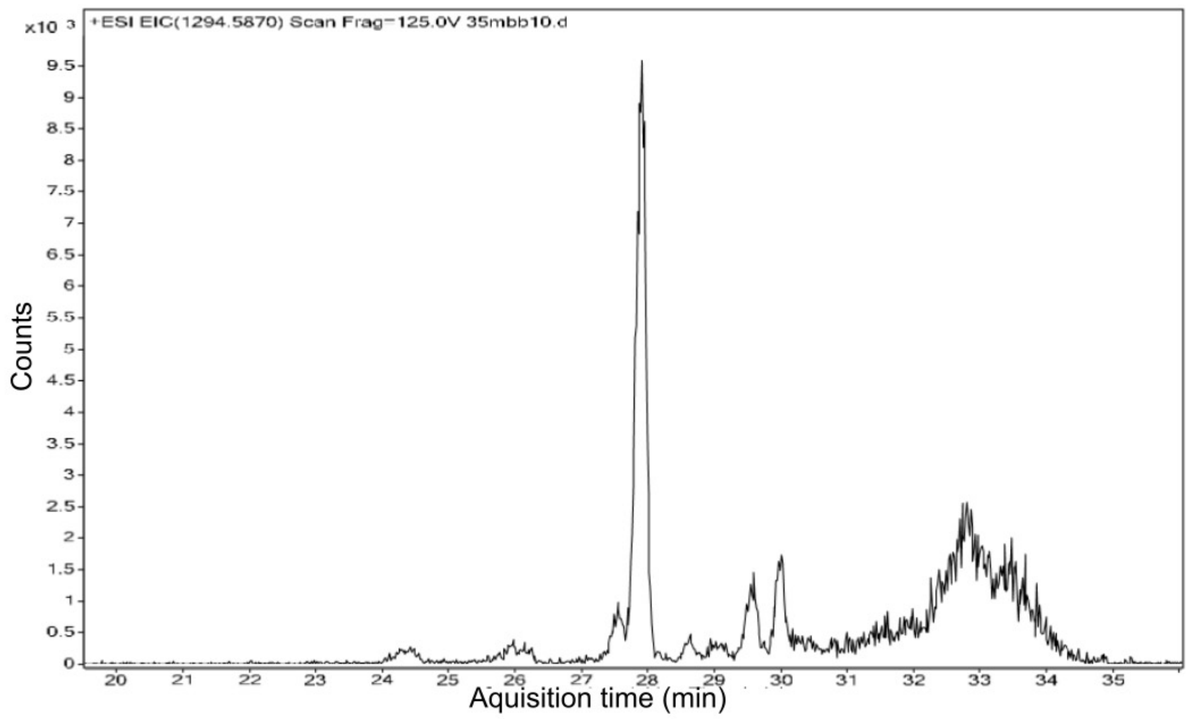

b

i

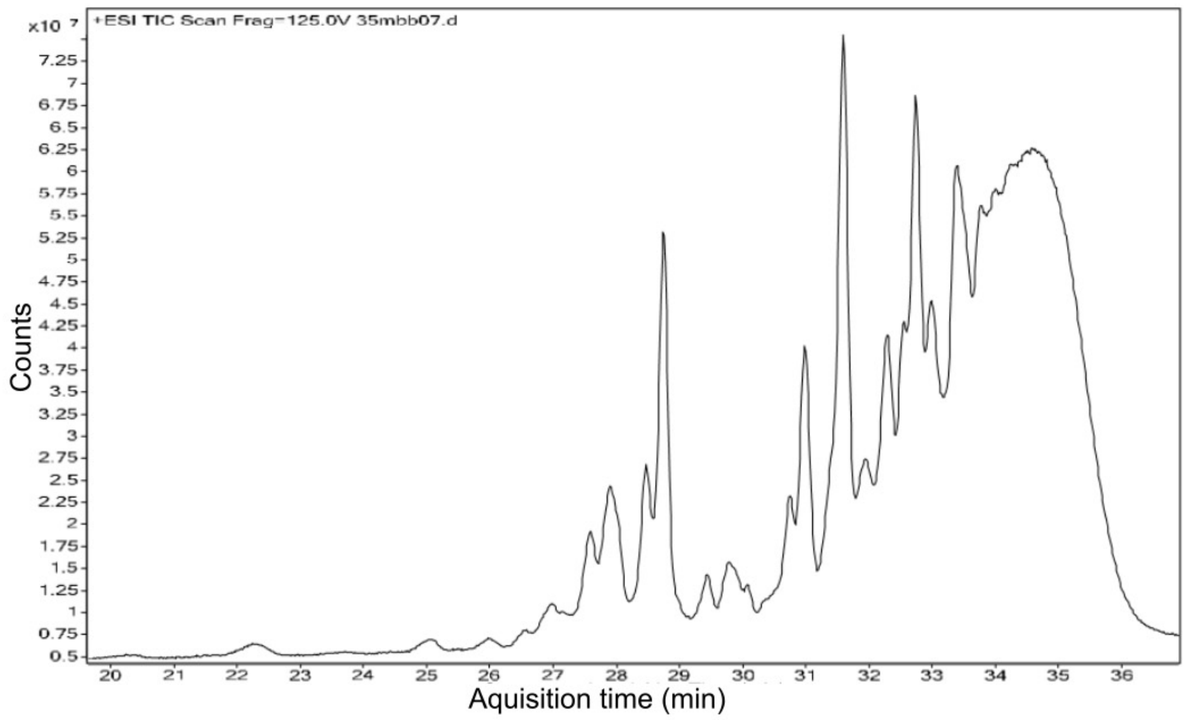

ii

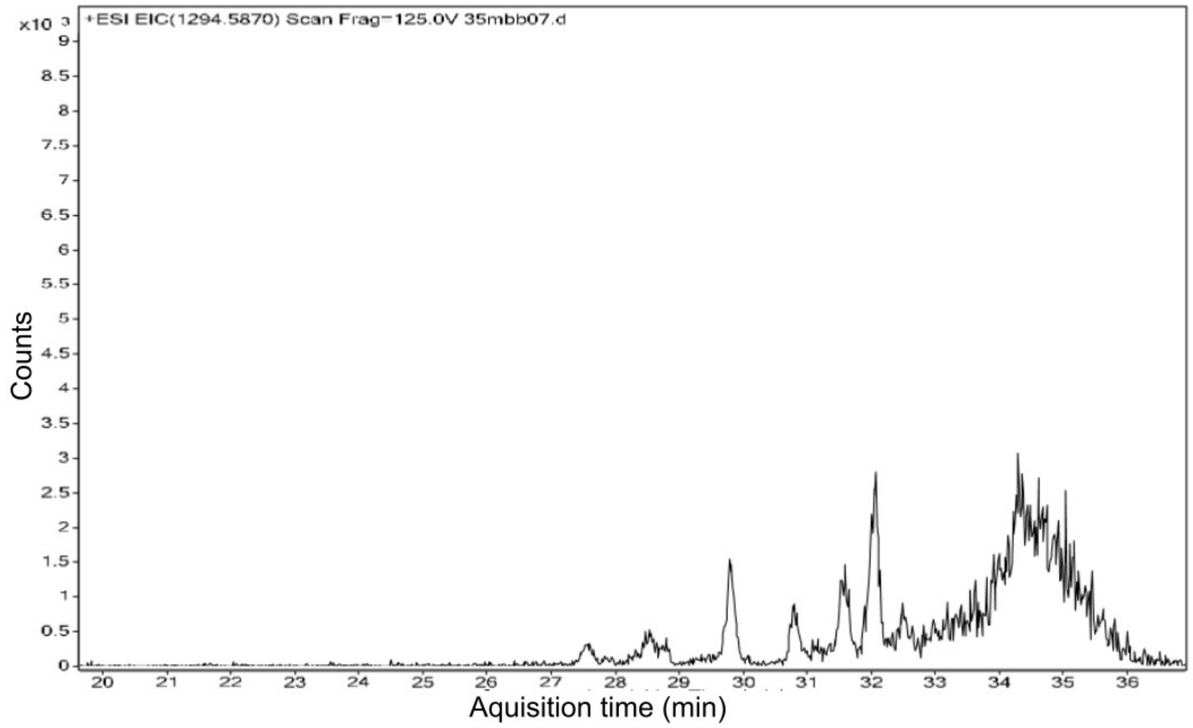

C

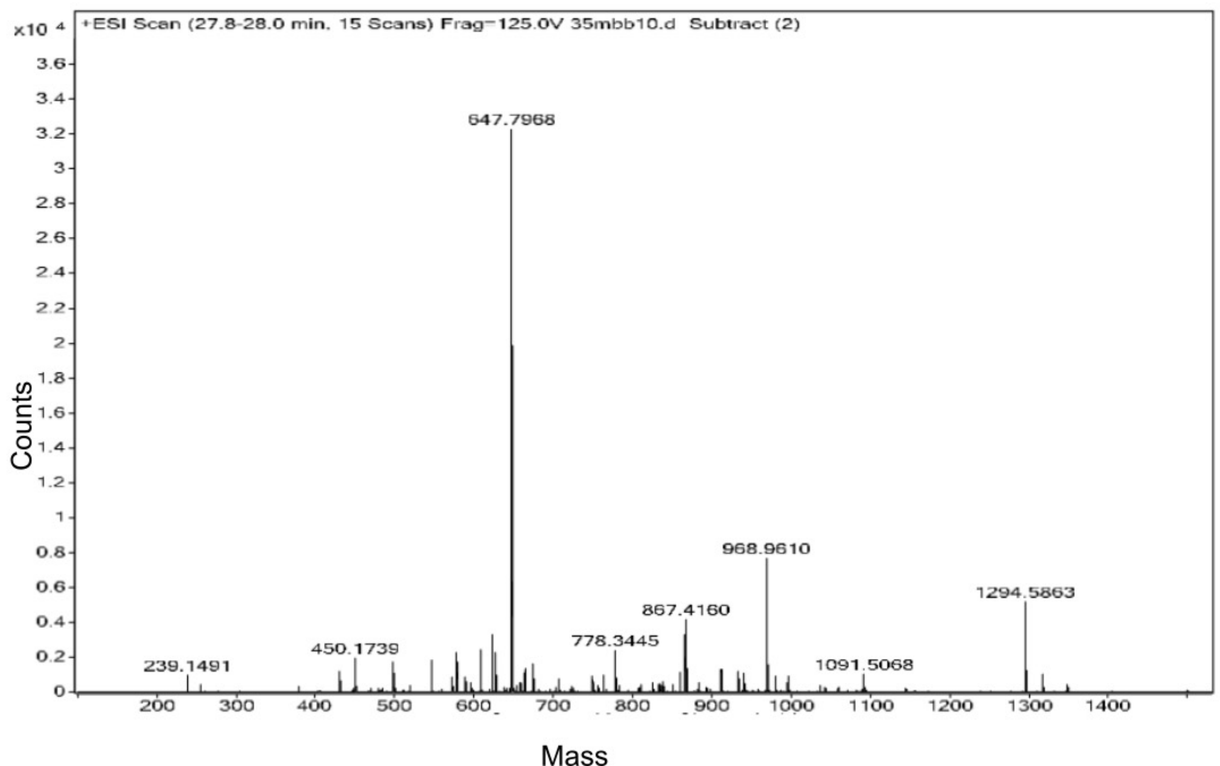

a

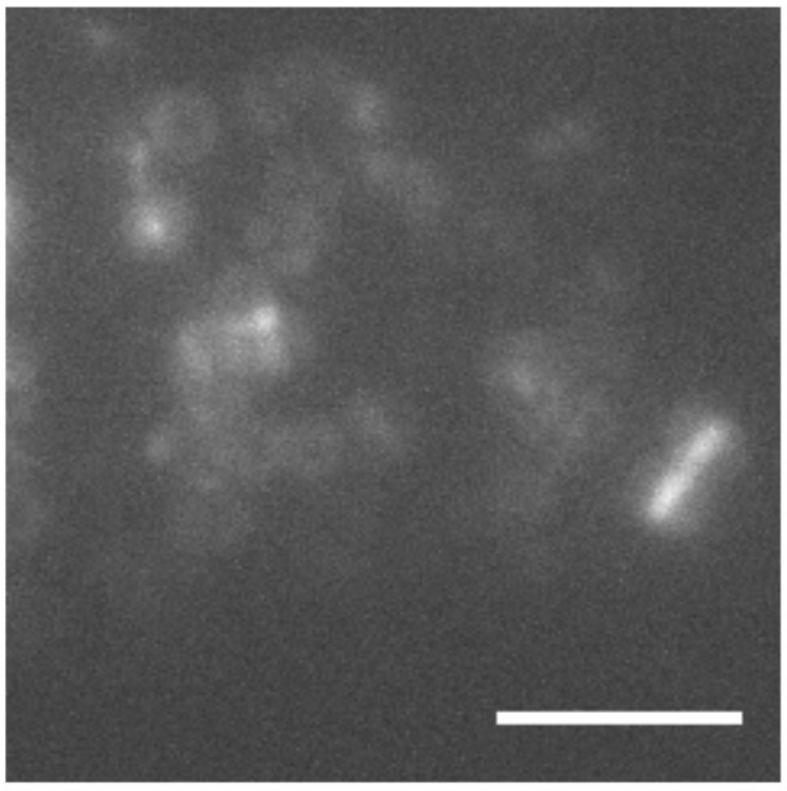

b i

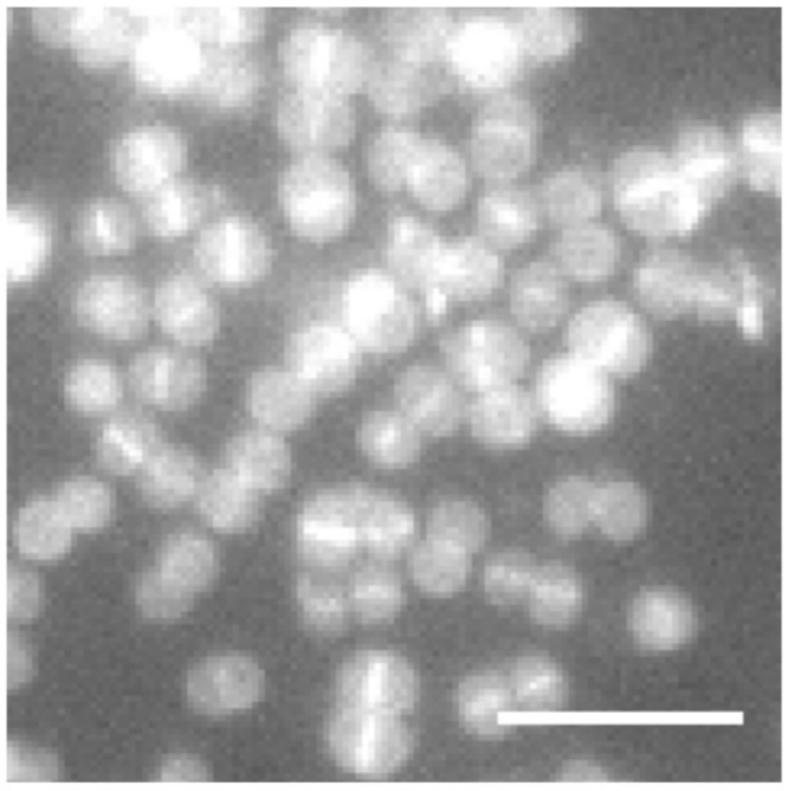

ii

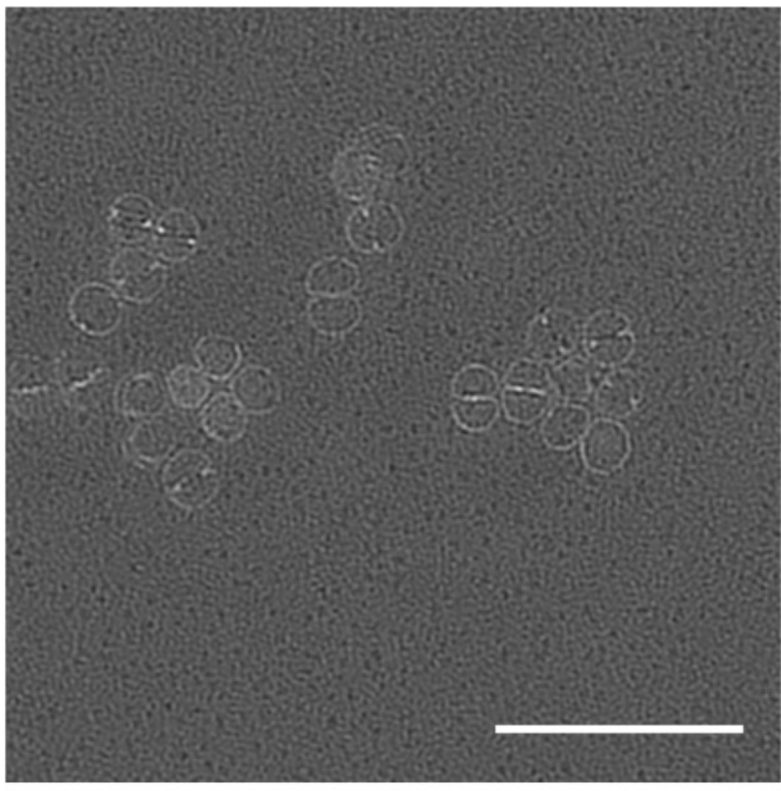

c i

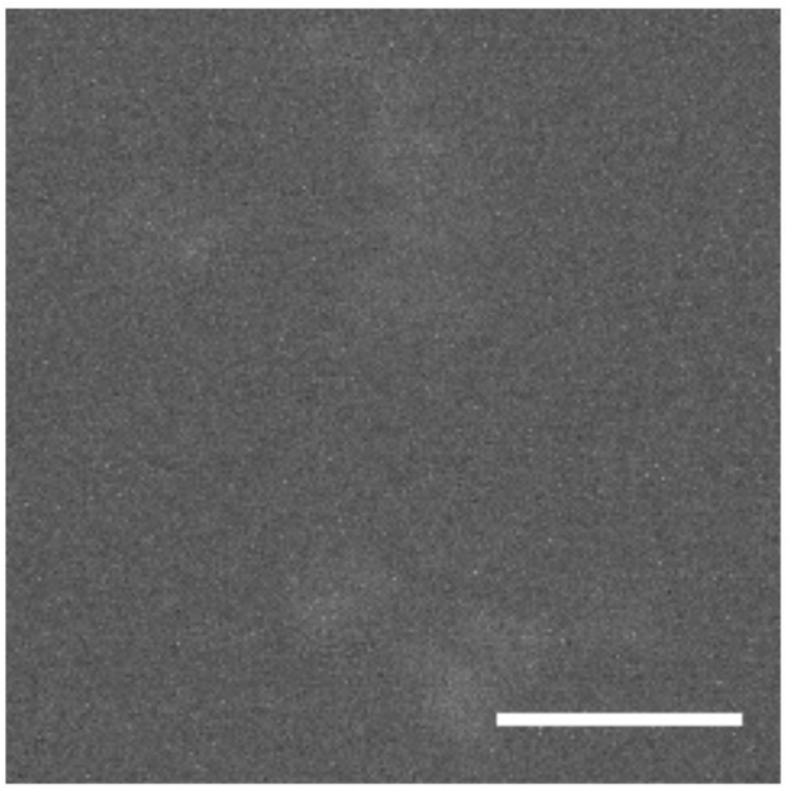

ii

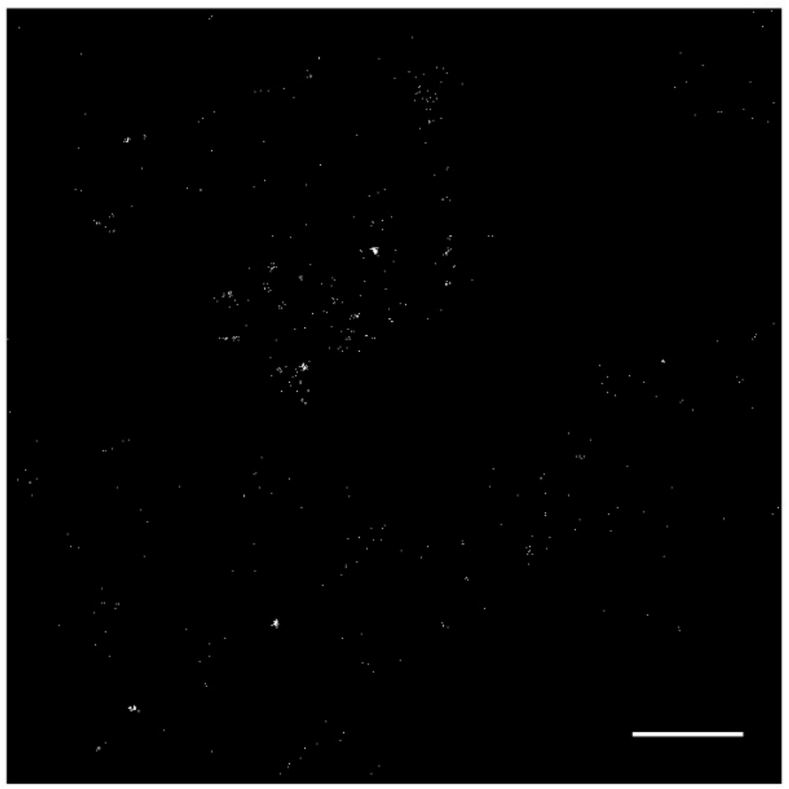

d

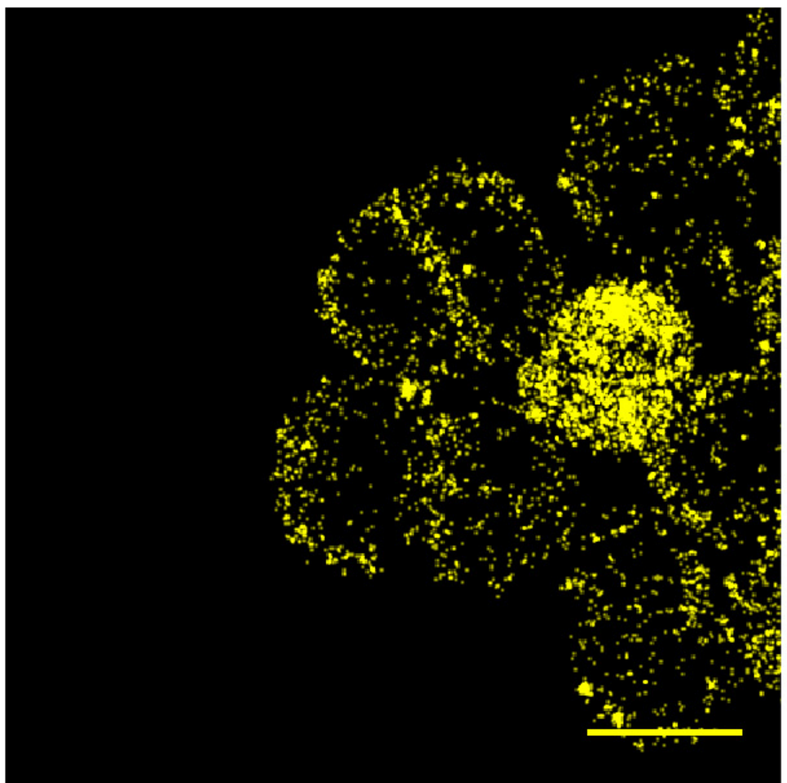

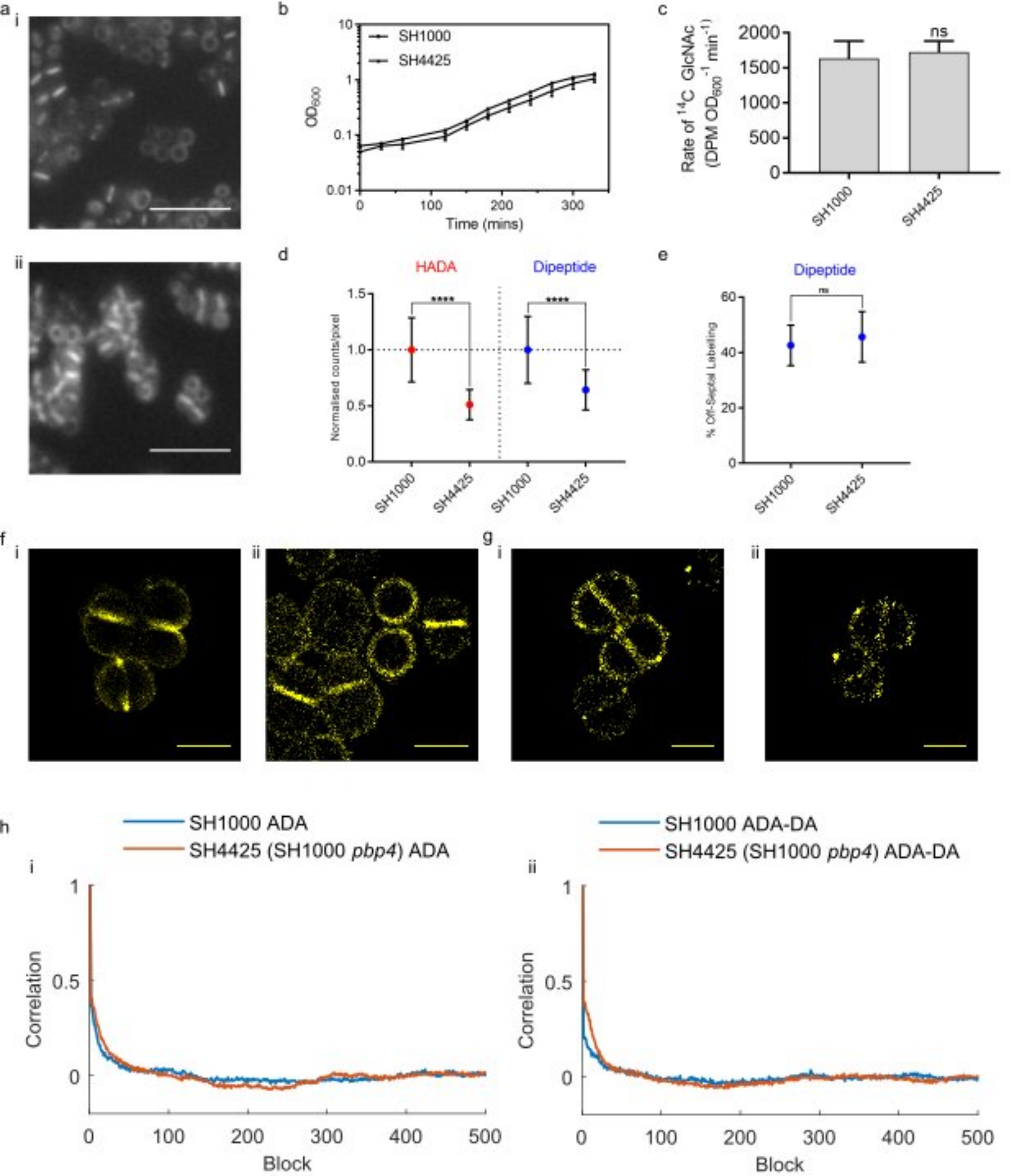
a
i
ii
b
SH1000
SH4425
OD600
Time (mins)
c
Rate of 14C GlcNAc (DPM OD600 -1 min-1)
ns
SH1000
SH4425
d
HADA
Dipeptide
Normalised counts/pixel
****
****
SH1000
SH4425
SH1000
SH4425
e
Dipeptide
% Off-Septal Labeling
ns
SH1000
SH4425
f
i
ii
g
i
ii
h
SH1000 ADA
SH4425 (SH1000 pbp4) ADA
SH1000 ADA-DA
SH4425 (SH1000 pbp4) ADA-DA
i
ii
Correlation
Block

a

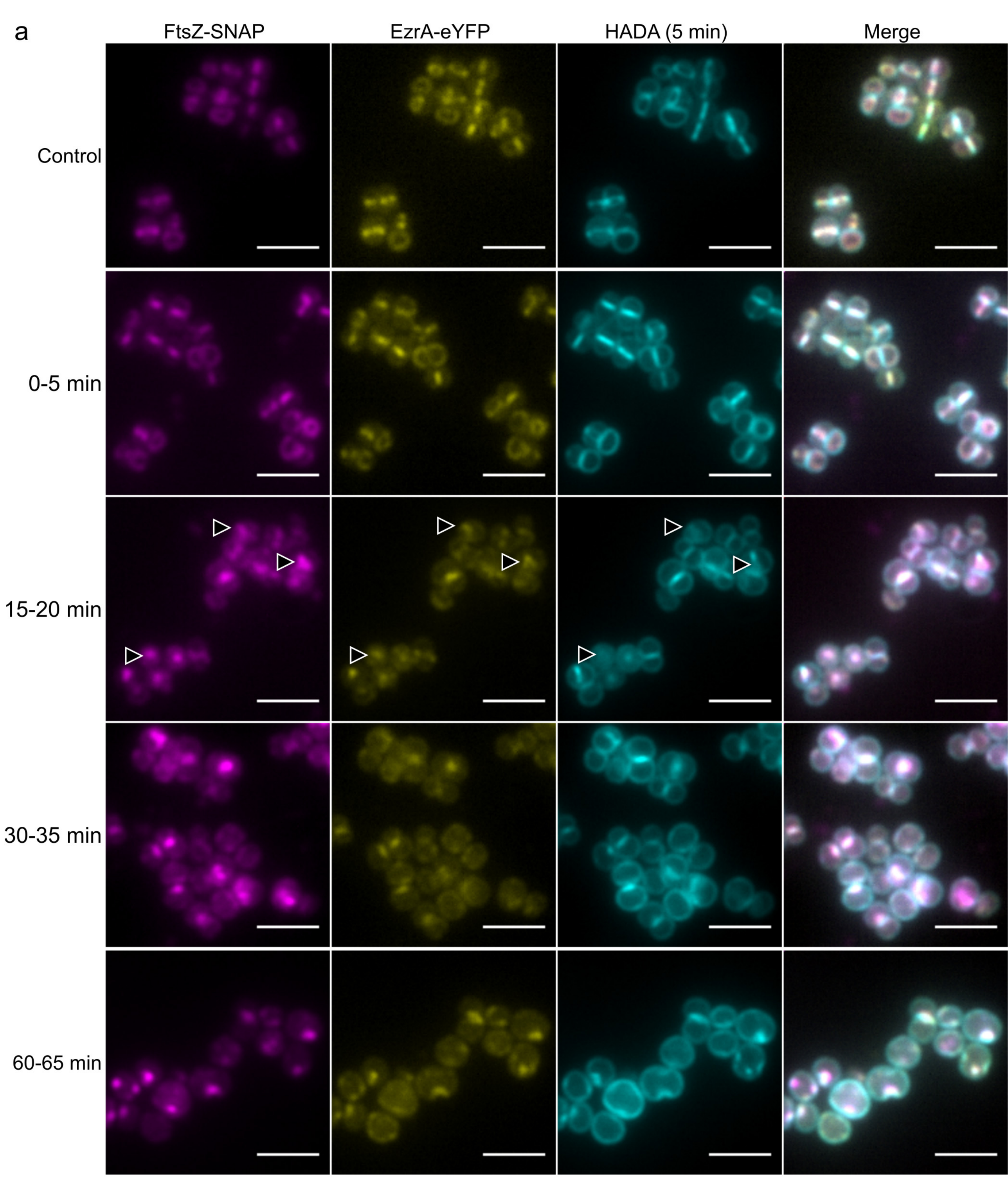
FtsZ-SNAP
EzrA-eYFP
HADA (5 min)
Merge
Control
0-5 min
15-20 min
30-35 min
60-65 min

b

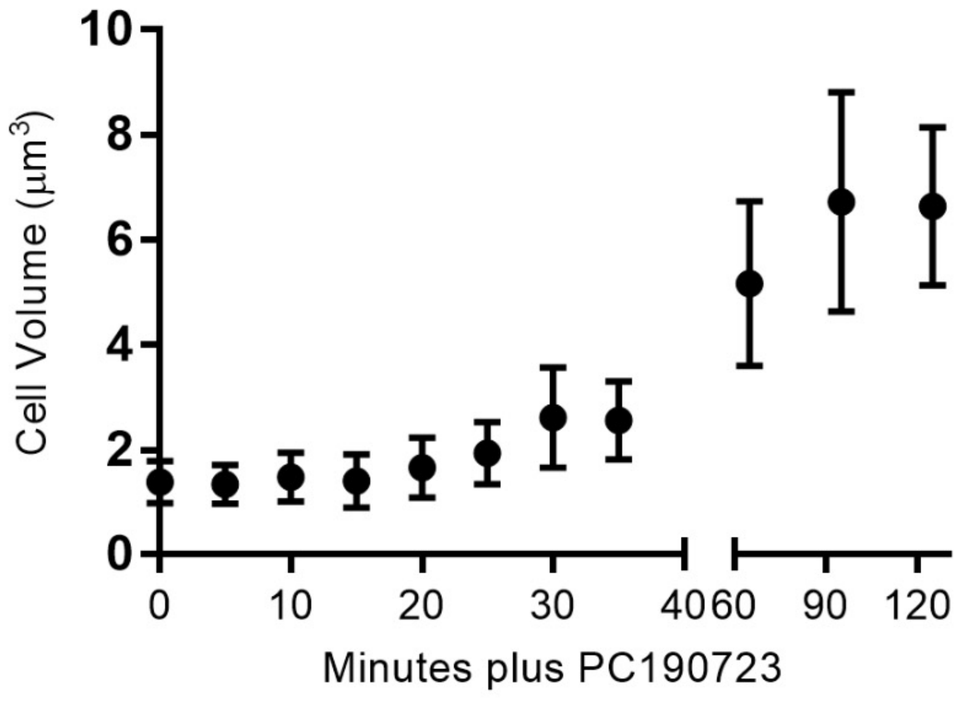
Cell Volume (µm3)
0
2
4
6
8
10
0
10
20
30
40
60
90
120
Minutes plus PC190723